China Geology 9 (2026) 102−119

China Geology

Journal homepage: http://chinageology.cgs.cn
https://www.sciencedirect.com/journal/china-geology

From amalgamation to post-orogenic Rodinian rifting: Decoded by the Neoproterozoic Shenshan Group, South China

Hong-shuai Wu[a, b], Yu-zhi Zhang[a, b, c,*], Xue Yang[d], Jian-wen Yang[c], Meng-yuan Li[a, b], Xiao-qing Yu[a, b], Cheng Wang[a, b], Cheng-shi Gan[a, b]

[a] *Guangdong Provincial Key Lab of Geodynamics and Geohazards, School of Earth Sciences and Engineering, Sun Yat-Sen University, Zhuhai* 519080, *China*
[b] *Southern Marine Science and Engineering Guangdong Laboratory (Zhuhai), Zhuhai* 519082, *China*
[c] *School of the Environment, University of Windsor, Windsor ON N9B 3P4, Canada*
[d] *China National Offshore Oil Corporation China Limited, Shenzhen Branch, Shenzhen* 518054, *China*

A R T I C L E I N F O

Article history:
Received 2 February 2024
Received in revised form 3 April 2024
Accepted 8 April 2024
Available online 14 April 2025

Keywords:
South China plate
Subdivision of the Shenshan Group
The upper Shenshan Subgroup
Sedimentary rock
Intermediate-acidic igneous source material
Post-orogenic rift setting
Meso-Neoproterozoic
Fore-arc environment
Rodinian continental rifting
Geological survey engineering

A B S T R A C T

The Shenshan Group provides important geological information which is vital in unraveling the amalgamation and subsequent rifting processes of South China. While conventional studies have asserted its formation in a subduction setting, the distinct investigation reveals the necessity for reassessment. To address this, the authors employ integrated methods encompassing petrological, zircon U-Pb geochronological, Lu-Hf isotopic and geochemical methods for sedimentary rocks from the upper Shenshan subgroup and Banxi Group. The geochemical results indicate that they were formed through the recycling deposition of intermediate-acidic igneous source material and experienced moderate chemical weathering. Additionally, both sedimentary sequences exhibit characteristics consistent with those formed in an intracontinental extensional rift setting since ca. 810 Ma. The provenance analysis indicates that the upper Shenshan subgroup primarily originates from the Yangtze Domain, while the Banxi Group from both the Yangtze and Cathaysia domains. Synthesizing with previous studies, the Shenshan Group should be subdivided into the lower and upper subgroups which represent distinct tectonic backgrounds. The lower subgroup is inferred to have formed in an Early Neoproterozoic fore-arc setting, akin to the Zhoutan group. The upper subgroup corresponds to the Banxi Group, representing the Middle Neoproterozoic post-orogenic rift setting, responding to the breakup of Rodinia.

©2026 China Geology Editorial Office.

1. Introduction

The South China Block (SCB, Fig. 1a) was formed through the amalgamation of the Yangtze and Cathaysia domains along the Jiangnan Orogen in the Neoproterozoic (Zheng YF et al., 2008; Wang YJ et al., 2013, 2019, 2024; Zhang YZ et al., 2013, 2015, 2020; Zhao GC, 2015; Yao JL et al., 2019; Shu LS et al., 2021). Numerous studies have focused on the spatio-temporal framework of its amalgamation process in SCB and paleogeographic reconstruction in Rodina (Li ZX et al., 1995, 2023; Li WX et al., 2005; Zhao JH et al., 2011; Zhang YZ et al., 2013, 2015; Wang XL et al., 2014; Shu LS et al., 2021; Wang YJ et al., 2024). The researches demonstrated a long-lived Neoproterozoic (ca. 970–830 Ma) Proto-Huanan arc-trench system at the periphery of Rodinia, extending southward to the South Delhi Fold Belt in a westerly-convergent manner (Wang YJ et al, 2013, 2024; Yao JL et al., 2019). An angular unconformity represented by a series of deformational, metamorphic and depositional geological characterization is underlain by the Lengjiaxi Group and its equivalents with characteristics of an arc-back-arc system (Wang YJ et al. 2013, 2019, 2024; Zhang YZ et al., 2013; Wang XL et al., 2014; Zhang YZ and Wang YJ, 2016, 2020). This angular unconformity is commonly regarded as the result of the orogenic event linked to the ultimate assembly of the Yangtze and Cathaysia domains (Wang J et al., 2003; Zhang YZ et al., 2015). Conversely, less attention has been paid to the timing and post-orogenic process of the SCB (Wang XL et al., 2012). Divergent viewpoints exist regarding the tectonic affinity (mantle plume-rifting versus plate-rifting) and the

First author: *E-mail address*: wuhsh23@alumni.sysu.edu.cn (Hong-shuai Wu).

* Corresponding author: *E-mail address*: zhangyuzhi@mail.sysu.edu.cn (Yu-zhi Zhang).

Literary editor: Li-qiong Jia
doi:10.31035/cg2024018
2096-5192/© 2026 China Geology Editorial Office.

Copyright © 2026 Editorial Office of China Geology. Publishing services by Elsevier B.V. on behalf of KeAi Communications Co. Ltd.
This is an open access article under the CC BY-NC-ND License (http://creativecommons.org/licenses/by-nc-nd/4.0/).

initial post-orogenic time of the SCB (about 850 Ma versus about 825 Ma versus 790 Ma vs Early Paleozoic) (Li XH et al., 1999; Wu RX et al., 2006; Zheng YF et al., 2008; Zhao JH et al., 2011; Wang YJ et al., 2013, 2019, 2024; Lin SF et al., 2018; Yao JL et al., 2019). In addition to clarifying the mechanisms involved in intracontinental reworking and elucidating the subsequent abundant granitic magmatism and mineralization processes (Wang YJ et al., 2013; Yu PP et al., 2019; Zheng Y et al., 2022), understanding the timing and process of the post-orogenic process is a vital link between the amalgamation of the SCB and the subsequent intracontinental orogenic events during the Phanerozoic (Wang YJ et al., 2013; Shu LS et al., 2021; Gan CS et al., 2024).

The disciplines of petrology and geochemistry serve as effective means for constraining tectonic settings. Predominantly, extant research has focused on investigations concerning igneous and metamorphic rock formations (Zhou

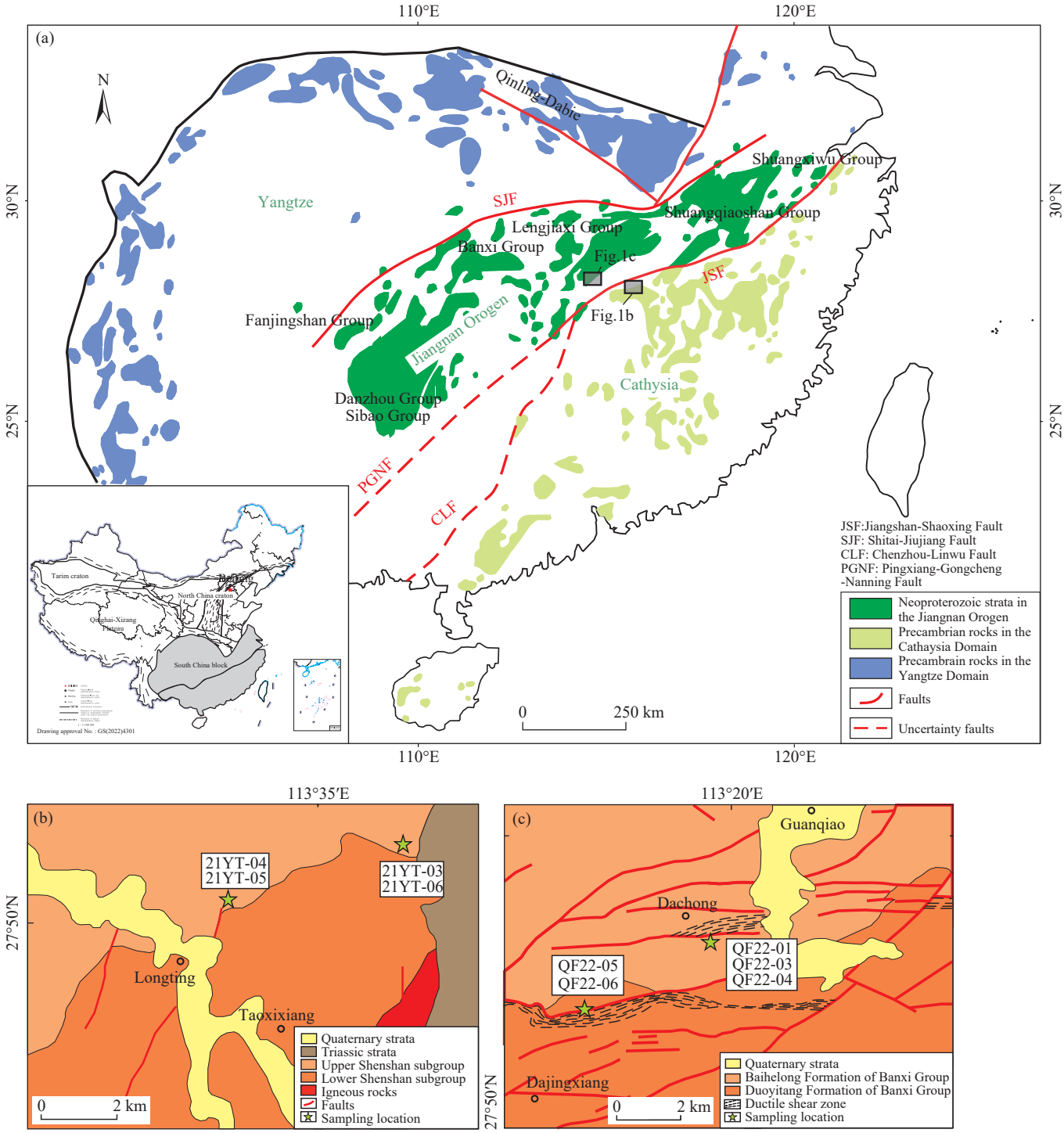

Fig. 1. Tectonic sketch map of Precambrian strata in South China Block (a, modified from Yang X et al., 2022 and Zhao GC and Cawood PA, 2012), simplified geological map of Yangtian Village in central Jiangxi Province (b, modified from Jiangxi BGMR, 1984) and Guanqiao Town in eastern Hunan Province (c, modified from Hunan BGMR, 1988).

JC et al., 2009; Wang YJ et al., 2019). Thus, to address these uncertainties, additional evidence from the geochemistry and detrital geochronology of sedimentary rocks related to the post-orogenic rifting process is required.

The Shenshan Group, located at the boundary between the Yangtze and Cathaysia domains, carries significance for their amalgamation and subsequent rifting process (Jiangxi BGMR, 1984). It has been broadly classified as a fore-arc basin setting produced in the subduction stage of the Proto-Huanan Ocean by studying the high-Mg volcanic and clastic rocks from the Shenshan Group (Wang KX et al., 2020; Wang LJ et al., 2022; Yang X et al., 2022). However, the recent investigation indicates that the upper Shenshan subgroup might not be formed in the subduction stage. In consequence, detailed stratigraphic subdivision is necessary to promote the filling of the research gap concerning the age determination and tectonic setting of the upper section of the Shenshan Group. Therefore, this study is focused on analyzing sedimentary rocks from the upper Shenshan subgroup and Banxi Group near the central Jiangnan Orogen. Through systematic field geological, petrological, zircon U-Pb geochronological, Lu-Hf isotopic, and whole-rock geochemical analyses of the sedimentary rocks, this article aims to determine the deposition age, provenance, and tectonic setting of the upper Shenshan subgroup in contrast with Banxi Group. Furthermore, the study underscores the necessity for a refined understanding of the tectonic evolution of the Shenshan Group, shedding light on its crucial role in elucidating the amalgamation and rift processes of the SCB. Additionally, this research will provide a foundation for the post-orogenic rift tectonic evolution of the SCB by employing a better-functioning discrimination method involving isometric log-ratio transformations and linear discriminant analysis.

2. Geological background

The Jiangnan Orogen is situated between the Yangtze and the Cathaysia domains, extending in an NNE direction for approximately 1500 km with a width of about 80–120 km. It can be subdivided into the eastern (Northwest Zhejiang, South Anhui, and Northeast Jiangxi), central (Northwest Jiangxi and West Hunan), and western segments (Northeast Guangxi and East Guizhou). This orogenic belt primarily comprises Neoproterozoic volcanic-sedimentary strata and contemporaneous magmatic rocks, which have undergone widespread low-grade metamorphism. Along the Jiangnan Orogenic belt, the basement is characterized by tight folding and deformation, mainly including the previously defined Meso- to Neoproterozoic Lengjiaxi Group and its equivalents (lower Shenshan subgroup, Shuangxiwu, Sibao, Fanjingshan, Shuangqiaoshan, and Xikou groups) (Hunan BGMR, 1988; Wang PM et al., 2012; Zhang YZ and Wang YJ, 2016, 2020; Yang X et al., 2022). The Banxi Group and its equivalents (Heshangzhen, Danzhou, Xiajiang, Dengshan, and Likou groups) show a relatively gentle stratigraphic sequence (Zhang QR et al., 2008; Gao LZ et al., 2011; Wang LJ et al., 2020). Throughout the regions, extensive exposures of Neoproterozoic granitic and mafic-ultramafic magmatic activities were observed (Wang LJ et al., 2022). The Lengjiaxi Gourp and its equivalents exhibit an unconformable relationship with the overlying Banxi and equivalent groups in the majority of the Jiangnan Orogen (Jiangxi BGMR, 1984; Hunan BGMR, 1988). This unconformity is widely accepted as a consequence of the orogenic event linked to the ultimate amalgamation of the Yangtze and Cathaysia domains (Wang YJ et al., 2019, 2024; Shu LS et al., 2021). It is worth noting that the unconformity is manifested by a sequence of volcanic rocks and volcanoclastic sedimentary breccias named Cangshuipu Group (Wang J et al., 2003; Zhang YZ et al., 2015).

The Shenshan Group is located in the northern part of Jiangxi Province, primarily exposed in the Yiyang–Fengcheng–Xinyu–Pingxiang region, with a total thickness of about 3500 m, predominantly consisting of pseudo-flysch clastic rocks and volcanoclastic rock assemblage (Jiangxi BGMR, 1984; Pan GT et al., 2016; Yang X et al., 2022). In the southern part, it is structurally in contact with sedimentary strata ranging from the Cryogenian to Ediacaran. While in the northern part, it unconformably underlies the Cretaceous or Quaternary sedimentary rocks. During the Kwangsian and Indosinian movements, the Shenshan Group underwent greenschist-facies metamorphism and was intruded by abundant granitic magmatism. Subsequently, these metamorphic rocks and granites were unconformably covered by Middle Devonian sedimentary rocks (Jiangxi BGMR, 1984; Wang LJ et al., 2022). In the Xinyu section, the lower stratigraphic unit is predominantly composed of carbonaceous and silty phyllite, interbedded with carbonaceous and metamorphic laminated sandstone. The upper section consists of gray-green sericite sandy phyllite and laminated siltstone, with a lesser proportion of carbonaceous sericite phyllite. In the Pingxiang–Dongqiao region, the lower section includes gray-green laminated fine sandstone and siltstone, interbedded with tuffaceous phyllite and meta-sedimentary tuff. The upper section is primarily composed of silty phyllite, accompanied by calcareous laminated siltstone, siliceous shale, and dolomitic limestone lenses. Additionally, various altered andesite and quartz porphyry developed in the Pingxiang–Dongqiao area. In the Fengcheng–Luoshi area, the lower part consists mainly of tuffaceous phyllite and tuffaceous shale sequences, interspersed with altered tuffaceous sandstone and variable thickness layers of altered fine-grained tuffaceous shale. The upper part is primarily composed of black carbonaceous shale, gray-green altered basalt, mate-andesite and volcanic breccia (Jiangxi BGMR, 1984). It can be observed that there are differences in lithology between the upper and lower sections of the Shenshan Group. In this study, we utilize the terms upper Shenshan subgroup and lower Shenshan subgroup to represent them respectively.

The Banxi Group is mainly distributed in the western and northern parts of the Hunan Province, with exposures in the

Qianyang–Xupu–Anhua–Xiangtan–Yuanling–Taoyuan–Guanqiao region. It has a thickness exceeding 3500 m, which decreases to less than 500 m towards the north within the craton interior (Fig. 1b). The Banxi and its equivalent groups are dominantly sedimentary packages characterized by well-developed greywackes, slates, greenschists and volcanoclastic rocks. It has experienced lower greenschist-facies metamorphism and exhibits well-preserved upright and open folds. The color transitions from predominantly reddish purple in the north to grayish-green and gray-black in the south. Based on lithological and facies characteristics, the Banxi Group is subdivided into Hengluchong, Madiyi, Tongtawan, Wuqiangxi, Duoyitang, Baihelong and Niuguping formations from bottom to top (Hunan BGMR, 1988). The samples from this study were collected from the Duoyitang and Baihelong formations. The Duoyitang Formation mainly comprises grayish-green and gray fine-grained slate, quartz mica schist, tuffaceous slate interbedded with tuffaceous sandstone and conglomerate tuff. The Baihelong Formation is mainly composed of conglomeratic feldspathic sandstone, feldspar-quartz sandstone, with minor occurrences of thin-bedded slate and tuffaceous slate. Research conducted on outcrops in regions such as Guzhang, Anjiang, Yuanling (West Hunan) and Shiershan (South Anhui) has constrained the formation age of the mafic-ultramafic rocks, tuffaceous rocks, and volcanic rocks within the range of about 809–711 Ma (Hunan BGMR, 1988; Gao LZ et al., 2011; Wang XL et al., 2012; Wang YJ et al., 2019).

3. Sample descriptions and analytical methods

This study collected sedimentary samples from the upper Shenshan subgroup near the Yangtian Village, Jiangxi Province (Fig. 1b, N27°42'44.25", E115°31'33.00"). The samples include quartz-mica slates (21YT-03 and 21YT-06) and meta-quartz sandstones (21YT-04, 21YT-04A, 21YT-04B, 21YT-04C and 21YT-05). Parallel bedding and overturned folds were observed at these locations (Figs. 2a, c, d). The mineral composition mainly consists of quartz (45%–50%), mica (muscovite, biotite, etc., 20%–30%), feldspar (mainly plagioclase 10%–20%, displaying aggregate twinning, Figs. 2c, d), and minor amounts of chlorite and magnetite as accessory minerals. They have moderate mineral grain size, with a relatively high degree of compositional maturity but poor sorting and rounding. Mica minerals exhibit a certain degree of directional structure, being elongated transversely and compressed longitudinally to form crystalline foliation (Figs. 2c, d). Overall, the samples from the upper Shenshan subgroup exhibit a schistose structure and flake recrystallization structure. Six samples were collected from the Banxi Group near Guanqiao Town, Hunan Province (Fig. 1c, N27°53'29", E113°19'15"). Among them, slate samples (QF22-01, QF22-02, QF22-03, QF22-04) and (QF22-05, QF22-06) were obtained from the Baihelong ($Ptbn_2l^3$) and Duoyitang ($Ptbn_2l^2$) formations of the Banxi Group. Both stratigraphic sedimentary layers at these locations have undergone subsequent shearing stress, forming ductile shear zones with an approximate dip angle up to 67° (Fig. 2b). These layers experienced low-grade metamorphism characterized by greenschist facies, with dominant minerals being feldspar and quartz, comprising over 80%, and containing minor amounts of muscovite and biotite (Figs. 2e, f).

This study presented whole-rock geochemical, detailed zircon U-Pb geochronology and Hf-O isotope analyses for the sedimentary samples in supplementary Tables S1−S3. Detailed analytical methods are presented in Appendix A.

4. Analytical results

4.1. Whole-rock geochemistry

The samples collected in this study are all clastic sedimentary rocks with a relatively low degree of metamorphism. Due to this limited metamorphic alteration, their chemical compositions are considered to closely reflect their original compositions. The results of the geochemical analysis conducted on these samples are listed in supplementary Table S1. For the seven samples from the upper Shenshan subgroup, the SiO_2 content ranges from 62.30% to 77.56%. Al_2O_3 varies from 14.64% to 20.48% with an average of 18.48%. Significant variations are observed in FeOt (2.23% to 7.65%) and MgO (0.73% to 2.78%), both showing consistent trends. The CaO content is relatively low, ranging from 0.06% to 0.56%, averaging at 0.28%. Except for one sample with a value of 0.19%, the Na_2O values for other samples vary from 0.82% to 2.44%. K_2O ranges from 3.03% to 4.93%. The Chondrite-normalized incompatible elements in the upper Shenshan subgroup show characteristics of high field strength elements (HFSE) depletion and enrichment of large ion lithophile elements (LILE) (Fig. 3a). The element Pb shows more enrichment, while Sr is more depleted. The Chondrite-normalized rare earth elements (REE) exhibit a subparallel and right-sloping distribution pattern with relatively enriched light rare earth elements (LREE) and relatively flat heavy rare earth elements (HREE) with $(La/Yb)_N$ = 11.61 and $(Gd/Yb)_N$ = 1.76 (Fig. 3b). Also, there is a negative Eu anomaly with Eu/Eu* = 0.23. The REEs exhibit similar patterns to those of the North American Shale Composite (NASC) and Post-Archean Australian Shale (PAAS) (Fig. 3b).

Six samples from the Banxi Group have SiO_2 contents ranging from 63.88% to 72.34%, with an average of 68.67%. Al_2O_3 varies from 14.9% to 20.8%, with an average of 17.9%. FeOt and MgO contents vary in the range of 4.65%–8.29% and 0.90%–1.50%, respectively. CaO content is very low, consistently between 0.059% and 0.065%. Na_2O content is extremely low. K_2O and TiO_2 contents are relatively high, ranging from 3.58% to 5.49% and 0.78% to 0.87%, respectively. The trace elements in the Banxi Group also exhibit characteristics of HFSE depletion and enrichment of LILE (Fig. 3c), with Pb being more enriched and Sr more depleted. The REE displays a subparallel and right-sloping

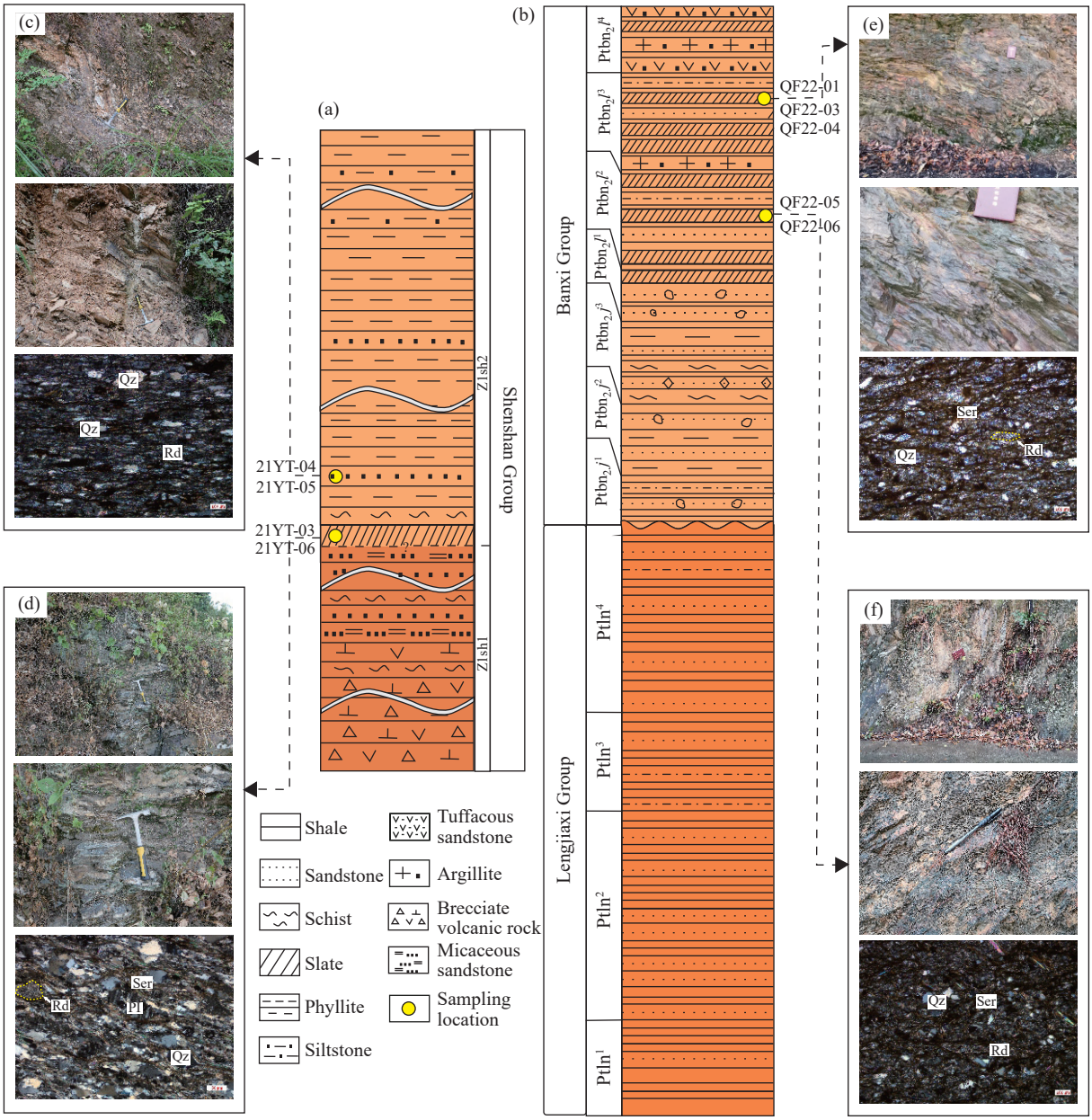

Fig. 2. Stratigraphic sequences of the Shenshan (a) and Banxi (b) groups (modified from Jiangxi BGMR, 1984; Hunan BGMR, 1988). Representative field and microscope photos showing the meta-quartz sandstone (c), quartz mica slate (d) of the upper Shenshan subgroup and the slate (e–f) of the Banxi Group.

distribution pattern with relatively enriched LREE and relatively flat HREE with $(La/Yb)_N$ = 10.66 and $(Gd/Yb)_N$ = 1.73 (Fig. 3d). The negative Eu anomaly is also shown with Eu/Eu* = 0.21, also resembling to those of NASC and PAAS (Fig. 3d).

4.2. Detrital zircon U-Pb geochronology and Lu-Hf isotopic analysis

Zircon U-Pb dating and Lu-Hf isotopic analysis were conducted on samples from two areas, including the quartz-mica slate (21YT-06) from the upper Shenshan subgroup, as well as the slates of the Baihelong (QF22-01) and Duoyitang formations (QF22-05) of the Banxi Group. The results of the analyses are presented in supplementary Tables S2 and S3, and cathodoluminescence (CL) images are shown in inserts in Figs. 4a, b, c. Zircon grains exhibit significant differences in size and mostly display euhedral to subhedral prismatic shapes, with a few showing moderately rounded subellipsoidal shapes. The Th/U ratios are consistently greater than 0.1, with the majority exceeding 0.3 (Fig. 4i), along with their typical oscillatory zoning, indicating a magmatic origin of the zircons (Hoskin PWO and Schaltegger U, 2003). The concordance of zircon ages is generally above 90% (Supplementary Table S2). For zircon grains younger than 1000 Ma, where the radiogenic Pb component has accumulated less and conventional Pb correction is challenging, the $^{206}Pb/^{238}U$ apparent age is used to represent the zircon crystallization age. For zircons older than 1000 Ma, where the radiogenic Pb has accumulated sufficiently, the

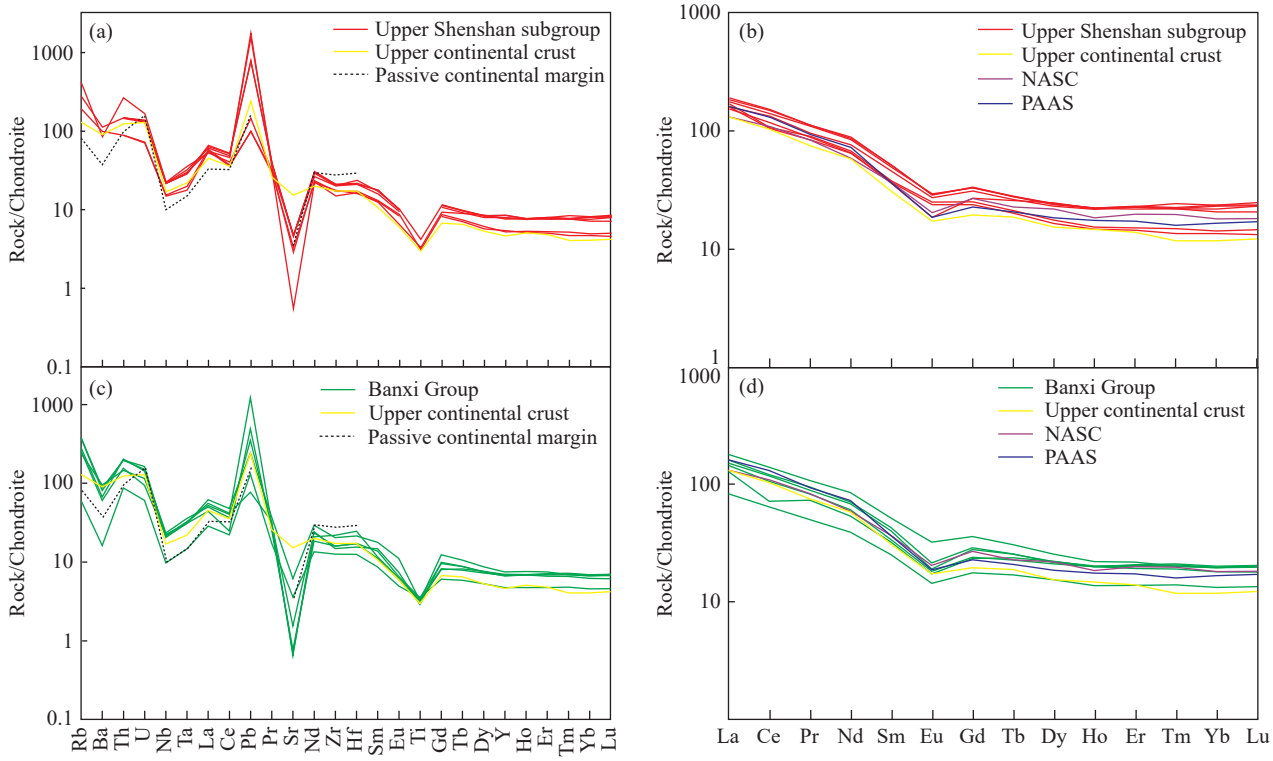

Fig. 3. Chondrite-normalized multi-element spidergrams and REE patterns for the sedimentary samples in the upper Shenshan subgroup (a, b) and Banxi Group (c, d). The values of chondrite, NASC and PAAS refer to Sun S and McDonough WF (1989) and Condie KC (1993).

$^{207}Pb/^{206}Pb$ apparent age is utilized to represent the zircon crystallization age (Cawood PA et al., 2012).

The zircon grains in sample 21YT-06 from the upper Shenshan subgroup are relatively large and exhibit uniform size, with length and width ranging between 100–150 μm (Fig. 4a). Analysis of 59 zircon points from this sample reveals a minimum apparent zircon age of 735±18 Ma, and the overall age spectrum spans from 3119 Ma to 735 Ma. The predominant age clusters are observed at 880–735 Ma, 2100–1800 Ma, and 2700–2400 Ma, with the minimum peak age at about 808 Ma (Fig. 4d). Frequency spectra for the youngest age interval (880–735 Ma) exhibit prominent age peaks at about 804 Ma and about 735 Ma (Fig. 4g).

Sample QF22-01 from the Banxi Group exhibits smaller zircon grains, with length ranging approximately from 30 μm to 80 μm and width from 20 μm to 50 μm (Fig. 4b). Among the 58 analyzed zircon grains, all U-Pb ages are concordant, with the minimum age peak at about 812 Ma (Fig. 4e). The overall age spectrum ranges from 3045 Ma to 718 Ma. Zircon grains in sample QF22-05 are slightly larger, with length around 60–120 μm and width around 30–80 μm (Fig. 4c). Analysis of 58 zircon grains from this sample reveals a minimum concordant age of 744±19 Ma, with the minimum age peak at about 786 Ma (Fig. 4f). The overall age spectrum spans from 2478 Ma to 744 Ma. Combining the zircon age data of the two samples, multiple age clusters are identified in the frequency spectra, including 900–700 Ma, 1300–1100 Ma, 1700–1400 Ma, 1900–1800 Ma, and 2600–2400 Ma of the Banxi Group. For the youngest zircon age range (about 900–700 Ma), a more detailed age-spectra pattern reveals two prominent age peaks at about 815 Ma and about 730 Ma (Fig. 4h).

For Lu-Hf isotopic analysis, 59 zircon grains from the upper Shenshan subgroup, which show concordant ages, were selected. The $^{176}Lu/^{177}Hf$ ratios range from 0.0001 to 0.0014, all of which are below 0.002. This suggests minimal accumulation of radiogenic Hf after zircon crystallization, and the measured $^{176}Hf/^{177}Hf$ values can represent the Hf isotopic composition of the system at the time of zircon formation (Wu FY et al., 2007). The Hf isotope variations are substantial (Fig. 5a), with $^{176}Lu/^{177}Hf$ ratios ranging from 0.280933 to 0.282574. The $\varepsilon_{Hf}(t)$ values span from −17.8 to +11.1, with 28 points being positive and 31 points negative. This indicates significant variations in the magmatic reservoir during zircon crystallization, suggesting characteristics both from a depleted mantle source and input of ancient crustal components. The two-stage model ages (T_{DMC}) range from about 3632 Ma to about 1016 Ma.

Lu-Hf isotopic analysis was conducted on 103 zircon grains from the Banxi Group, all of which exhibited concordant ages and well-preserved morphologies. The $^{176}Lu/^{177}Hf$ ratios range from 0.0003 to 0.0027, with the majority being below 0.002, indicating minimal accumulation of radiogenic Hf after zircon crystallization. The measured $^{176}Lu/^{177}Hf$ values represent the Hf isotopic composition of the system at the time of zircon formation. The Hf isotope compositions very widely (Fig. 5b), ranging from 0.280395 to 0.282588, and the $\varepsilon_{Hf}(t)$ values range from −28.0 to +14.9. Among these, 46 spots show positive $\varepsilon_{Hf}(t)$, and 57 show negative $\varepsilon_{Hf}(t)$, suggesting that the source material was

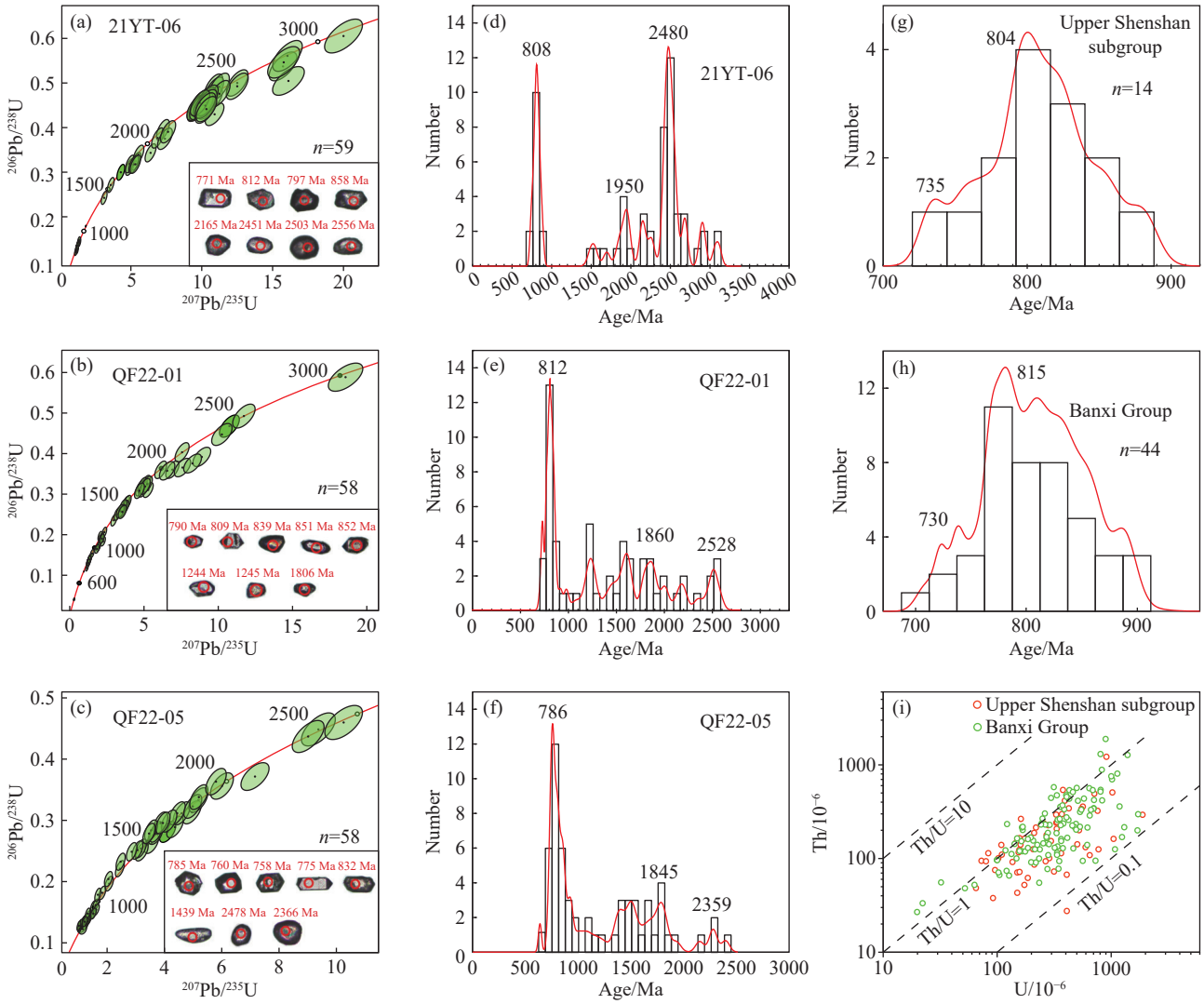

Fig. 4. Detrital zircon U–Pb concordia diagrams, age histograms for the sedimentary samples in the upper Shenshan subgroup (a, d, g) and Banxi Group (b, c, e, f, h) and the correlation between Th/U and age (i) for the analyzed zircons.

dominated by recycled ancient crustal components, with a limited contribution from the depleted mantle. Excluding the zircon point with an $\varepsilon_{Hf}(t)$ value of −28, the two-stage model ages (T_{DMC}) of the other zircons range from 3889 Ma to 881 Ma.

5. Discussion

5.1. Deposition age of the upper Shenshan subgroup and Banxi Group

The youngest detrital zircon U–Pb peak age in sedimentary rocks serves as a valuable tool for constraining the maximum sedimentary age for the sedimentary packages (Dickinson WR and Gehrels GE, 2009). In this study, the detrital zircon age spectrum of quartz-muscovite slate from the upper Shenshan subgroup exhibits a predominant peak at about 808 Ma (Fig. 6a). Meanwhile, Yang et al. (2022) determined that the age of the high-Mg volcanic rocks in the lower Shenshan subgroup is about 838 Ma. Consequently, the authors posit that the lower limit of sedimentation for the upper Shenshan subgroup occurred at about 810 Ma. A more detailed examination of the age spectrum within this interval revealed a minimum peak age of about 735 Ma (Fig. 4g). Gabbros in the upper Shenshan Group gave a zircon U-Pb age of 791±9 Ma (Wang LJ et al., 2020). The youngest detrital zircons in the upper Shenshan subgroup metavolcanic rock sequence fall within the range of about 790–740 Ma, with a peak at about 776 Ma (Wang LJ et al., 2020). Additional supporting evidence includes South Jiangxi potassic granulites with ages of about 774 Ma and about 756 Ma (Zhou BW et al., 2018). Furthermore, Jiang Y et al. (2019) obtained an age of about 734 Ma for the Nanping–Ninghua rhyolites. Collectively, these findings substantiate that the sedimentation of the upper Shenshan subgroup occurred between 810 Ma and 735 Ma.

The deposition ages of the Lengjiaxi and Cangshuipu groups along the Jiangnan Orogen have traditionally been constrained to be 860–830 Ma and 830–810 Ma, respectively (Wang J et al., 2003; Gao LZ et al., 2011; Wang XL et al., 2014; Zhang YZ et al., 2015; Zhang YZ and Wang YJ, 2016, 2020; Wang YJ et al., 2024). Detrital zircons analysis on the

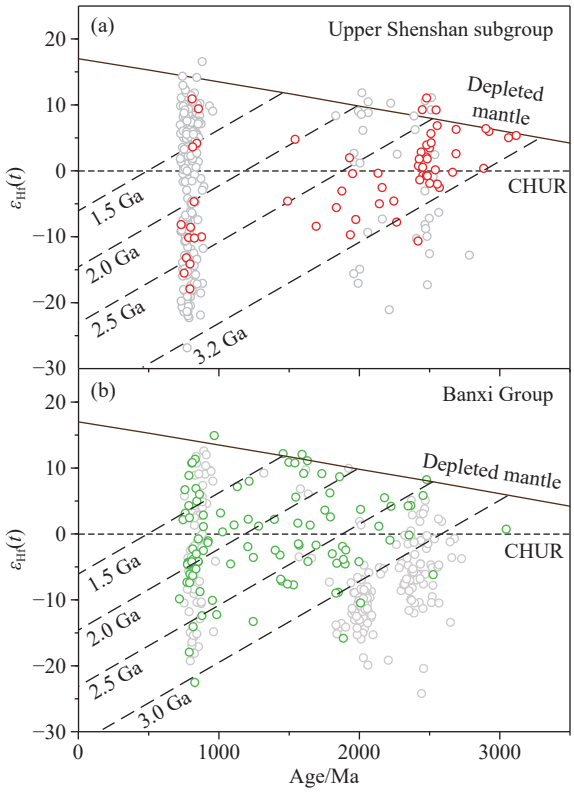

Fig. 5. Diagram of zircon U-Pb apparent ages versus $\varepsilon_{Hf}(t)$ values for the sedimentary samples from the upper Shenshan subgroup (a) and Banxi Group (b). Data for the upper Shenshan subgroup are from Wang LJ et al., 2020, 2022. Data for the Banxi Group are from Wang W et al., 2012, 2013; Wang JQ et al., 2017.

volcanoclastic sandstone layers yielded the youngest age range concentrated between 803–791 Ma, with a peak age of about 797 Ma, also supported by the zircons of tuff beds being about 803 Ma (Gao LZ et al., 2011). Moreover, reports from the Sanfang, Bendong, Xucun and Jiuling regions indicate that granites underlying the Banxi Group and its equivalents are dated at about 820 Ma (Zheng YF et al., 2007; Wang XL et al., 2014; Duan Z et al., 2018). The detrital zircons from the Banxi Group samples give the minimal peak age of about 805 Ma (Fig. 6b). Igneous rocks of 810–740 Ma (mainly 790–760 Ma) have been developed, such as Aikou-Qianyang alkaline basalt, Yuanling-Anjiang gabbro-diabase, A-type and S-type granites in different regions (Li WX et al., 2005; Wu RX et al., 2006; Zheng YF et al., 2008; Cawood PA et al., 2012; Wang YJ et al., 2013, 2018, 2019, 2024). The above evidence collectively suggests that the sedimentation of the Banxi Group started at about 810 Ma at the earliest. By replotting the detrital zircon age spectrum of Banxi Group samples with ages between 880–720 Ma, the youngest age peak value obtained is about 730 Ma (Fig. 4h). Additionally, the youngest concordant age of detrital zircons in Banxi Group samples is 718±17 Ma. Detrital zircons from the volcanoclastic sandstone of the Niuguping Formation in Zhijiang (Hunan) gave the youngest age peak at about 725 Ma (Zhang QR et al., 2008). it can be inferred that the sedimentation time of the Banxi Group lasted until at least about 720 Ma. Therefore, the deposition age of the Banxi Group is refined to the interval of 810–720 Ma and shares similarities to the upper Shenshan subgroup.

5.2. Geochemical constraints on the weathering process and source rock material

Complex processes occur during the diagenesis of sedimentary rocks, necessitating a thorough analysis of their weathering degree. According to the classification diagram of terrestrial sandstones, the samples mainly fall into the categories of greywacke and arkose (Supplementary Fig. S1), consistent with the microscopic mineral characteristics. This observation suggests minimal long-distance transportation of the source rocks. Moreover, the significant presence of zircon grains within the 890–740 Ma range, coupled with the well-preserved and low-roundness property of the zircon grains (Fig. 4), supports the inference that the samples represent proximal deposition (Pettijohn FJ et al., 1972).

The Chemical Index of Alteration (CIA) was proposed as an indicator reflecting the degree of weathering in the source region for sedimentary rocks (Nesbitt HW and Young GM, 1982). CIA is calculated as follows: $CIA=\{x(Al_2O_3)/[x(Al_2O_3)+x(CaO^*)+x(Na_2O)+x(K_2O)]\}\times 100$. Here, CaO represents the amount of CaO in silicate minerals, i.e., the molar fraction of CaO in the whole rock minus that in carbonate and phosphate minerals, with CaO* representing the amount of CaO after correction for apatite. With the increase of CIA values, there is a corresponding rise in both the temperature and humidity under weathering conditions (Wollast R and Chou L, 1992). The CIA values for samples from the upper Shenshan subgroup and Banxi Group range from 72.6 to 81.5 and 78.5 to 80.5, respectively, both indicating an intermediate degree of chemical weathering intensity under warm and humid conditions (Fig. 7a), also supported by the negative anomaly features of Sr in the spidergram (Figs. 3a, c; Green TH, 1994). During the processes of transportation, deposition, and diagenesis, alterations in rock composition may arise, particularly attributed to potassium alteration, which is notably observed in Precambrian clastic rocks. It is mainly manifested by the reaction of minerals such as aluminite with potassium ions in pore water, resulting in the formation of illite (Nesbitt HW and Young GM, 1982). The introduction of external potassium ions can disrupt the expected weathering trend of rocks, causing deviation towards the corner with higher potassium content, as illustrated by line C in Fig. 8b. In this study, samples from the upper Shenshan subgroup show a similar weathering trend, while those from the Banxi Group deviate from the weathering trend and instead trend towards the corner enriched in K_2O in the ternary plot (Fig. 8a), indicating a significant potassium alteration.

Another important parameter used to determine whether sedimentary rocks have undergone recycling processes is the Index of Compositional Variability (ICV). The potassium alteration during diagenesis in clastic rocks can alter the original composition of the rocks. Therefore, when calculating the ICV value, it is necessary to correct for potassium

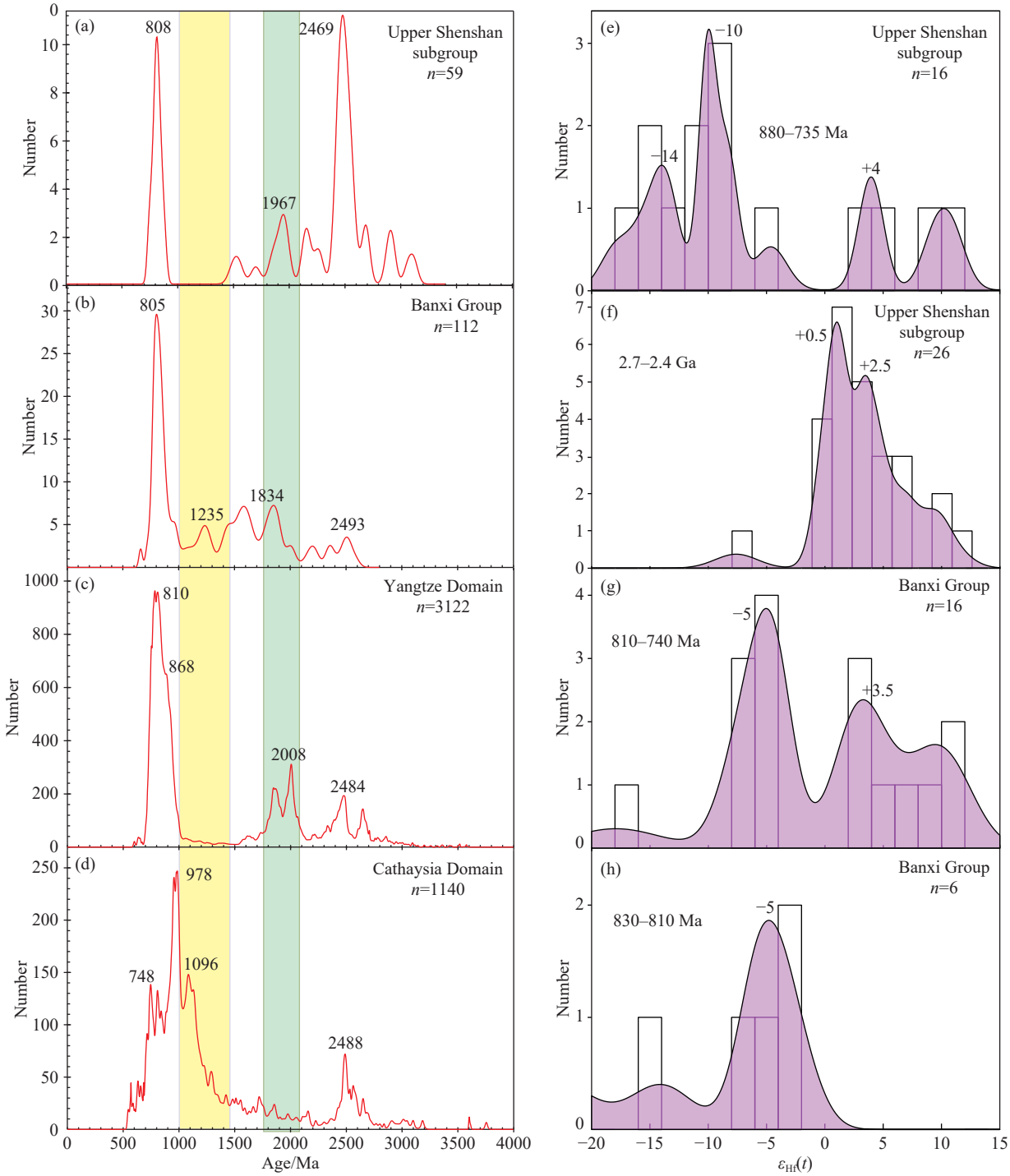

Fig. 6. Synthetical histograms of initial Hf isotope ratios and detrital zircon U-Pb ages for the metasedimentary rocks from the upper Shenshan subgroup (a), Banxi Group (b), Yangtze Domain (c) and Cathaysia Domain (d), and relative probability density diagrams of zircon $\varepsilon_{Hf}(t)$ values for the metasedimentary rocks from the upper Shenshan subgroup (e, f) and the Banxi Group (g, h). Data for the Yangtze Domain are from Greentree MR et al., 2006; Liu XM et al., 2008; Sun WH et al., 2009; Hofmann M et al., 2011; Wang W et al., 2012, 2013; Cui X et al., 2014; Lan ZW et al., 2015; Chen Q et al., 2016. Data for the Cathaysia Domain are from Wan YS et al., 2007; Yu JH et al., 2008, 2010; Wu L et al., 2010; Xu XB et al., 2010; Wang PM et al., 2012, 2013; Wu H et al., 2013; Gao LZ et al., 2014; Wang JQ et al., 2017.

alteration. The formula for calculating ICV is as follows: ICV = $[n(Fe_2O_3) + n(K_2O^*) + n(Na_2O) + n(CaO^*) + n(MgO) + n(MnO) + n(TiO_2)]/n(Al_2O_3)$; $K_2O^* = n(K_2O, \text{sample}) - n(K_2O, \text{added})$, here $n(K_2O, \text{added}) = [mA + m(C + N)]/(1-m)$, $m = K/(A+C+N+K)$ (A, C, N, K represent the molar fractions of Al_2O_3, CaO, Na_2O, and K_2O, respectively). CaO* only represents the CaO in silicates, and K_2O^* is the corrected K_2O.

When the ICV of sedimentary rocks is greater than 1.0, it indicates that the rocks contain few clay minerals, suggesting their first deposition in a tectonically active zone (Ronadh C et al., 1995). On the contrary, the rocks might have undergone redeposition processes or deposited for the first time under strong chemical weathering conditions. The ICV values for

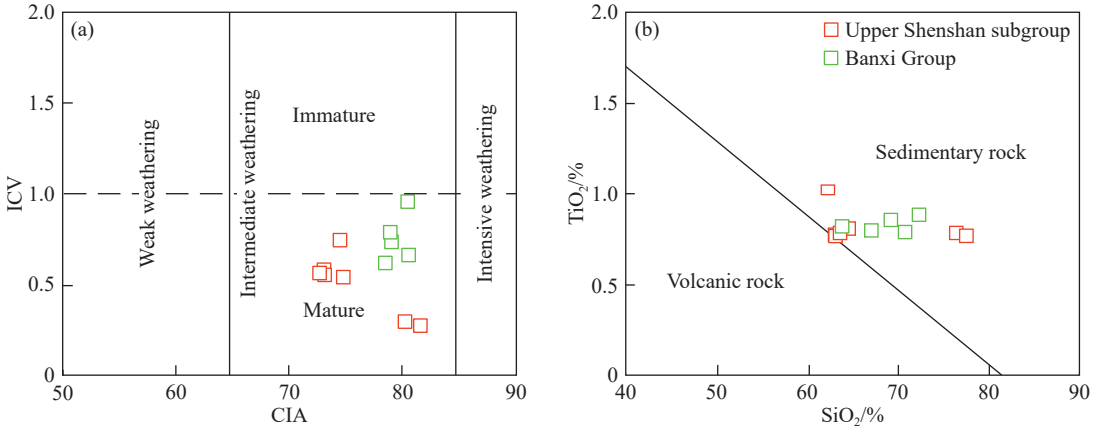

Fig. 7. Discrimination diagrams of the degree of weathering (a) and source rock (b) for the sedimentary samples in the upper Shenshan subgroup and Banxi Group (modified from Nesbitt HW and Young GM, 1982 and Hugh R, 1993).

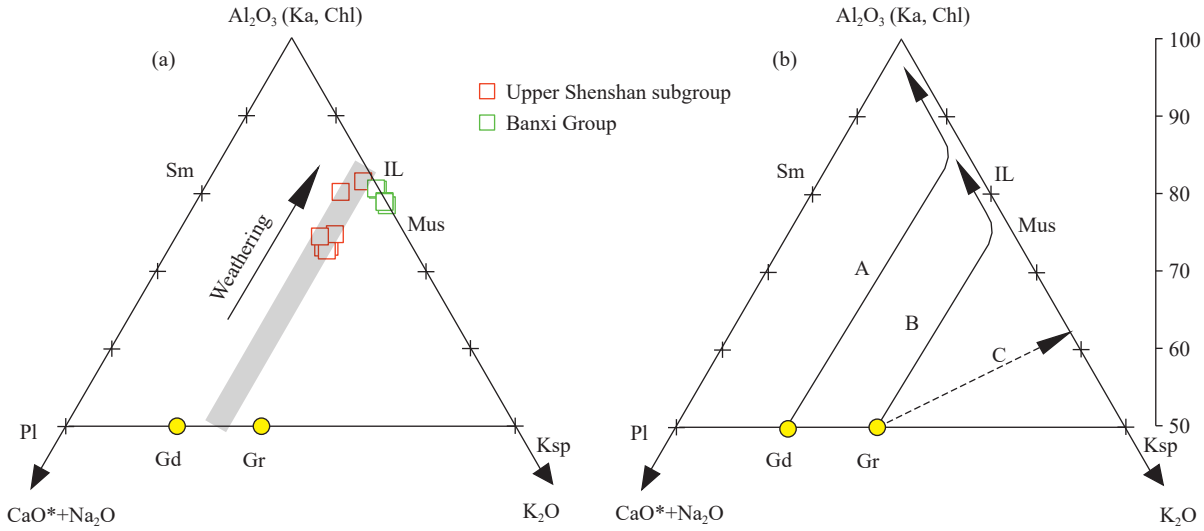

Fig. 8. Diagrams of A–CN–K triangulation (a) and the trend of chemical weathering and potassium replacement (b) for the metasedimentary samples in the upper Shenshan subgroup and Banxi Group (modified from Nesbitt HW and Markovics G, 1997 and Alireza P et al., 1999). A–Chemical weathering trend line of Toorongo granodiorite; B–normal weathering trend line of Ville Marie granite; C–deviation of the weathering trend line of Ville Marie granite due to K substitution reaction. Ka–kaolinite; Chl–chlorite; IL–illite; Mus–muscovite; Pl–plagioclase; Sm–smectite; Ksp–K-Feldspar; Gd–granodiorite; Gr–granite.

the upper Shenshan subgroup samples are relatively low, ranging from 0.27 to 0.58, while the Banxi Group samples have relatively high ICV values, ranging from 0.62 to 0.96, both being less than 1.0 (Fig. 7a). Additionally, in the SiO_2–TiO_2 source rock discrimination diagram, their original rock types fall within the sedimentary rock range, indicating that both groups of samples may have undergone a redeposition process (Fig. 7b). Similarly, the higher Zr/Sc ratio suggests that the rocks may have undergone zircon enrichment processes (Fig. 9a), reflecting the characteristics of redeposited sedimentary rocks.

During the chemical weathering process of the upper crust, elements such as Na and Ca are highly reactive. They are initially lost in ionic form with surface fluids, forming minerals like illite and muscovite mica under favorable conditions. The highly active K element gradually undergoes loss with the progression of weathering, forming minerals such as kaolinite and chlorite. During this process, the Al_2O_3 content in weathering products increases continually, while the molar fractions of CaO, Na_2O, and K_2O gradually decrease. Therefore, the A–CN–K ternary diagram can be utilized to judge the source rock composition by the weathering trend (Fig. 8). Generally, in ideal weathering conditions, elements in granite (Gr) and granodiorite (Gd) evolve with a decrease in CaO+Na_2O content followed by a decrease in K_2O content (Fig. 8b; Nesbitt HW and Markovics G, 1997; Alireza P et al., 1999). The Al_2O_3-(CaO*+Na_2O)-K_2O ternary diagram shows that the weathering trend of the upper Shenshan subgroup samples is similar to the ideal condition (Fig. 8a). Therefore, based on the weathering trend, it is inferred that the chemical composition of their source rocks should be between granodiorite and granite. Additionally, in the discrimination diagram for major elements of provenance (Fig. 9d), upper Shenshan subgroup samples are placed between the felsic igneous rocks and quartzite sedimentary rocks of source regions. Trace elements

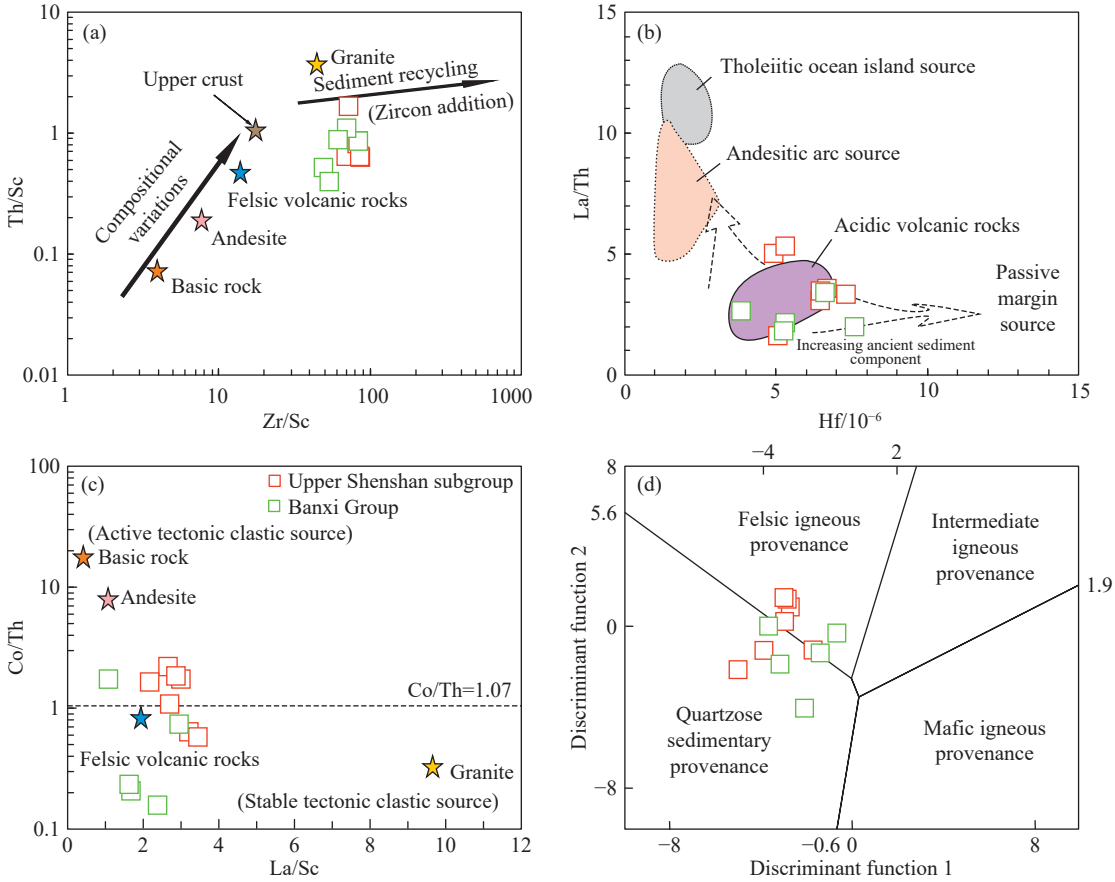

Fig. 9. Source composition discrimination diagrams of Zr/Sc *vs*. Th/Sc (a, after McLennan SM et al., 1989), Hf *vs*. La/Th (b, after Floyd PA and Leberidge BE,1987), La/Sc *vs*. Co/Th (c, after Condie KC, 1993) and discriminant function 1 *vs*. discriminant function 2 (d, after Roser BP and Korsch RJ,1988) for the metasedimentary samples from the upper Shenshan subgroup and Banxi Group. Discriminant function 1 = $-1.773TiO_2 + 0.607Al_2O_3 + 0.76Fe_2O_3 - 1.5MgO + 0.616CaO + 0.509Na_2O - 1.224K_2O - 9.09$; Discriminant function 2 = $0.445TiO_2 + 0.07Al_2O_3 - 0.25Fe_2O_3 - 1.142MgO + 0.438CaO + 1.475Na_2O + 1.426K_2O - 6.861$.

have low mobility during the sedimentary process and have a short residence time in the ocean, making them effective indicators for identifying sediment sources. Generally, HFSEs (such as Th, Zr, Hf and Ti) and REEs are mainly enriched in felsic minerals, while transition elements such as Sc, V and Co, are more enriched in mafic minerals (Taylor SR and McLennan SM, 1985). Therefore, clastic rocks from a felsic igneous rock source have lower Co/Th values and higher Th/Sc and La/Sc ratios. In the Th/Sc–Zr/Sc diagram (Fig. 9a), the upper Shenshan subgroup samples are close to the path of sedimentary cycling from felsic volcanic rocks to granite, away from the basaltic end-member, indicating characteristics of a felsic volcanic rock source, which is also reflected from the characteristics in the Co/Th–La/Sc diagram (Fig. 9c). Elements La, Th and Hf are stable during the sedimentary process and are favorable evidence for identifying source rock characteristics (Dickinson WR et al., 1983). The upper Shenshan subgroup samples also fall within the acidic rock source region in the La/Th–Hf correlation diagram (Fig. 9b). Therefore, the comprehensive evidence suggests that the provenance for the upper Shenshan subgroup samples mainly originates from intermediate-acidic magmatic rocks of the source. For samples from the Banxi Group, the same diagrams show characteristics of a felsic magmatic source. However, in the discrimination diagram for major elements in the provenance, they mainly fall within the quartzite sedimentary rock source region (Fig. 9d). We infer that it might be caused by the potassium alteration effect on Banxi Group samples, resulting in an increase in K_2O content and a relative decrease in Na_2O and CaO content. This causes the values of the discrimination function to decrease. Therefore, the source rock for the Banxi Group samples also comes from intermedium-acidic rocks, similar to those of the upper Shenshan subgroup.

5.3. Provenance of the sedimentary sequences

The Yangtze and Cathaysia domains underwent different evolution processes and tectonic events in the Precambrian. The Yangtze Domain generally underwent crustal growth and magmatic events at 2.9–2.4 Ga, 2.05–1.85 Ga, and 920–800 Ma, corresponding to age peak values of about 2.5 Ga, about 2.0 Ga, and about 0.81 Ga, coupled with the Paleoproterozoic orogeny related to the assembly of the Columbia supercontinent and the Neoproterozoic magmatic activity, respectively (Fig. 6c; Li XH et al., 1999, 2012; Zhou MF et al., 2002; Liu XM et al., 2008). The Cathaysia Domain mainly experienced Late Archean (2.6–2.5 Ga) crustal growth and the

Grenville Orogeny (1.3–0.9 Ga), represented by detrital zircon age peak values of about 2.5 Ga and about 1.0 Ga, respectively (Fig. 6d; Yu JH et al., 2008, 2010; Wang W et al., 2012). By comparing the detrital zircon age spectrum characteristics of both domains (Figs. 9c, d), it can be observed that the Yangtze Domain has characteristic age peaks at 2.0–1.8 Ga, while the Cathaysia Domain shows unique detrital zircon age distribution characteristics of 1.3–0.9 Ga.

The detrital zircon age spectrum of our upper Shenshan subgroup samples exhibits a notable absence of zircons falling within 1500–900 Ma range of the Grenville orogenic period (Fig. 6a). This deviation contrasts with the typical detrital zircon spectrum distribution pattern observed in the Cathaysia Domain (Fig. 6a) but aligns more closely with the age distribution shown in the Yangtze Domain (Fig. 6c). The primary detrital zircon age peaks are concentrated at 880–735 Ma and 2.7–2.4 Ga (Fig. 6a). The $\varepsilon_{Hf}(t)$ values for 880 Ma–735 Ma zircons range span from −17.8 to +11.0, with peak values declining in the order of −10, −14 and +4 (Fig. 6e). Notably, all $\varepsilon_{Hf}(t)$ values for zircons ranging from 810 Ma to 735 Ma are negative, and the second-stage model ages (T_{DMC}) range from 2826 Ma to 2168 Ma, significantly older than their crystallization ages. It is inferred that the source rocks experienced partial melting during the Late Archean to the Paleoproterozoic. Furthermore, the $\varepsilon_{Hf}(t)$ values for zircons within 880–810 Ma range predominantly exhibit positive values, resembling those of arc volcanic rocks formed in a subduction setting during this temporal interval (Zhou JC et al., 2009; Zhang YZ et al., 2013; Wang XL et al., 2014; Zhang YZ and Wang YJ, 2016, 2020). This concordance strongly suggests these zircons likely originated from arc magmatism that prevailed during this period. The $\varepsilon_{Hf}(t)$ values for about 2.7–2.4 Ga zircons are mainly concentrated between −2.5 and +11.1, mostly positive (Fig. 6f), closely aligning with the trend of depleted mantle evolution. The majority of zircons are situated between two crustal evolution lines at 3.2 Ga and 2.6 Ga (Fig. 5a), indicative of a significant episode of new crustal growth occurring between 3.2–2.6 Ga. This finding is in accordance with the results reported by Li XH et al. (2012) from zircon Hf isotope analysis with the same age range for the Yangtze Domain. There is currently no compelling evidence to suggest a comparable occurrence of new crustal growth in the Cathaysia Domain during the Late Archean. Additionally, the $\varepsilon_{Hf}(t)$ peak values for 2.7–2.4 Ga zircons are recorded at −0.5 and 2.5 (Fig. 6f), similar to those for the about 2.7–2.6 Ga zircons ($\varepsilon_{Hf}(t)$ ranging from 0 to +7.93) measured by Chen K et al. (2013) in the Kongling TTG and granite-porphyry of the Yangtze Domain. This similarity strongly suggests a high probability that the Archean material from the Yangtze Domain contributed part of the source for the upper Shenshan subgroup. In summary, the provenance of the upper Shenshan subgroup is predominantly derived from the Yangtze Domain.

The comprehensive U-Pb age spectrums for our samples reveal the presence of zircons between 1.3–0.9 Ga in the Banxi Group (Fig. 6b), indicating that part of the provenance for the Banxi Group might be the Cathaysia Domain (Fig. 6d). In more detail, the detrital zircon age spectrum in the Banxi Group is most abundant in the 880–720 Ma age range, forming a single-peaked distribution (Fig. 6b). Further analysis reveals that the 880–830 Ma zircon ages are similar to the minimum peak ages of the Lengjiaxi Group and its equivalents (Zhou JC et al., 2009; Wu L et al., 2010; Wang XL et al., 2014; Zhang YZ et al., 2015), suggesting recycling sedimentation from these groups. The 830–810 Ma zircons have negative $\varepsilon_{Hf}(t)$ values, with a peak value of −5 (Fig. 6h), consistent with the reported about 825 Ma granite ($\varepsilon_{Hf}(t)$ value of −3.4±0.8) in the Sanfang region of the western Jiangnan Orogen (Zheng YF et al., 2007), proving that the main provenance may come from the basement rocks and granites of the Jiangnan Orogen. The 810–740 Ma zircons exhibit a positive $\varepsilon_{Hf}(t)$ peak value of +3.5 (Fig. 6g), consistent with the dual-peak intrusive rocks ($\varepsilon_{Hf}(t)$ value of 3.5±0.8) in the Kangdian Rift of the west Yangtze Domain at 760–750 Ma (Zheng YF et al., 2007). Additionally, its detrital zircon spectrum contains a peak age of about 1800 Ma (Figs. 9b, c), which matches the characteristic age peaks of the Yangtze Domain. The evidence jointly suggests that the detrital zircons in the Banxi Group originate from both the Cathaysia and Yangtze domains.

6. Tectonic implications

6.1. Early Neoproterozoic post-orogenic rifting model in the SCB

The differentiation between active and passive continental margins is crucial for academic and economic development (Dickinson WR and Suczek CA, 1983). In the realm of geochemical studies, despite research has predominantly focused on igneous and metamorphic rocks, there has been notable progress in investigating the geochemistry of sedimentary rocks to provide relevant insights. Through comprehensive investigations, the tectonic setting was able to be reconstructed by analyzing the geochemical composition of terrestrial sediments (Nesbitt HW and Young GM, 1982; Bhatia MR, 1983; McLennan SM et al., 1989; Floyd PA et al., 1991; Robert LC and Victor NP, 2002). From the chondrite-normalized spidergrams (Fig. 3a, c), it can be observed that the trace element abundances of the upper Shenshan subgroup and Banxi Group closely resemble those of the passive continent margin (Floyd PA et al., 1991). Especially, elements such as Nb, Ta, and Sr exhibit depletion relative to the continental crust, while Ti, Hf and Zr enrichment in line with the passive continent margin model. The positive anomalies observed in Zr and Hf can be attributed to the enrichment of heavy minerals, primarily zircon, during mineral separation in a passive continental margin setting (Watson EB and Harrison TM, 1984; Dostal J and Chatterjee AK, 2000). In the chondrite-normalized REE patterns (Figs. 3b, d), the variations in REE contents of our samples exhibit a remarkable similarity to those of NASC and PAAS. This

parallel further strengthens the argument for their tectonic background as a passive continental margin (Taylor SR and McLennan SM, 1985; McLennan SM et al., 1989).

In recent years, the assessment of the tectonic origins of sedimentary basins has commonly employed binary or ternary diagrams based on major trace elements of sedimentary rocks (Bhatia MR, 1983; Bhatia MR and Crook KAW, 1986). Despite the widespread application, binary or ternary diagram projections sometimes suffer the issue of exhibiting nearly constant or consistently constant results (Verma SP and Armstrong AJS, 2016). Furthermore, inaccuracies and uncertainties in the analyzed data can introduce distortions, amplifications, or reductions in visual perceptions within ternary diagrams (Verma SP and Armstrong AJS, 2016). Therefore, a more accurate discrimination method employing isometric log-ratio transformations (ilr) has been suggested (Verma SP and Armstrong AJS, 2016). The transformed data of samples from active continental margin associated with Pacific subduction-collision settings are converted into isometric log-ratio proportion forms, and utilizing parameters for linear discriminant analysis, undergoing a multivariate normal distribution, these data are then used to demarcate tectonic boundaries. Using this method, the success rates in distinguishing between active and passive continental margins range at 87%–97% and 84%–86%, respectively (Verma SP and Armstrong AJS, 2016). The formulas for individual major elements are as follows:

$$\begin{aligned} DF_{(A-P)M} = & 3.0005\times ilr1_{Tim}+2.8243\times ilr2_{Alm}-1.596\times \\ & ilr3_{FeM}-0.7056\times ilr4_{MnM}-0.3044\times ilr5_{MgM}+ \\ & 0.6277\times ilr6_{CaM}-1.1838\times ilr7_{NaM}+1.5915\times \\ & ilr8_{KM}+0.1526\times ilr9_{PM}-5.9948. \end{aligned} \quad (1)$$

The tectonic boundary $(A\text{-}P)_{boundary}$ is defined by subtracting the average value of the centroids of the active and passive continental margin groups (−0.078376).

The formulas for combination of major and trace elements are:

$$\begin{aligned} DF_{(A-P)MT} = & 3.2683\times ilr1_{TiMT}+5.3873\times ilr2_{AlMT}+ \\ & 1.5546\times ilr3_{FeMT}+3.2166\times ilr4_{MnMT}+ \\ & 4.7542\times ilr5_{MgMT}+2.0390\times ilr6_{CaMT}+ \\ & 4.0490\times ilr7_{NaMT}+3.1505\times ilr8_{KMT}+ \\ & 2.3688\times ilr9_{PMT}+2.8354\times ilr10_{CrMT}+ \\ & 0.9011\times ilr11_{NbMT}+1.9128\times ilr12_{NiMT}+ \\ & 2.9094\times ilr13_{VMT}+4.1507\times ilr14_{YMT}+ \\ & 3.4871\times ilr15_{ZrMT}-3.2088. \end{aligned} \quad (2)$$

The tectonic boundary $(A\text{-}P)_{boundary}$ defined by this formula is −0.13345. A more detailed account of the calculation procedure was illustrated in Verma SP and Armstrong AJS. (2016).

The applications of this discriminant formula to samples from the upper Shenshan subgroup and Banxi Group yield a range of $DF_{(A-P)M}$ values from −14.38 to −1.20, all falling below zero. Additionally, $DF_{(A-P)MT}$ values varying from −0.60 to 8.32, With the exception of three samples displaying slightly negative values, all others exhibit values greater than zero (Fig. 10). These results distinctly indicate the presence of a passive continental margin tectonic setting.

The continental margin encompasses various tectonic settings at different stages. Passive continent margins comprise various scenarios such as Atlantic-type rifted continental margins, sedimentary basins on trailing continental margins supplied from collision orogens, and inactive or extinct convergent plate margins (Bhatia MR and Crook KAW, 1986). During the Early Neoproterozoic, approximately until 830 Ma, the SCB experienced an accretionary orogenic event along the periphery of Rodinia, leading to the amalgamation of the Yangtze and Cathaysia domains (Wang YJ et al., 2013, 2019, 2024; Zhang YZ and Wang YJ, 2016, 2020). The process involved a series of soft collisions lacking deep continental subduction and high-grade metamorphism typically associated with continent-continent collisions (Zhao GC, 2015). Along the Jiangnan Orogen, evidence of Neoproterozoic magmatic rocks (830–740 Ma), primarily represented by S-type granites and OIB-type basalts (Zheng YF et al., 2008; Wang YJ et al., 2019), contradicts the tectonic setting of trailing continental margins and inactive or extinct convergent plate margins. The development of Atlantic-type rifted continental margins normally contains three stages: the pre-rift stage characterized by intracontinental basins, the rift valley stage marked by widespread subsidence of continental crust, and the post-breakup stage with the onset of mid-ocean ridges and rifted oceanic crust (Falvey DA, 1974). Detrital zircons ages of 830–810 Ma and 810–740 Ma in this study, originating mainly from S-type granites and bimodal igneous rocks respectively, were associated with pre-rift and syn-rift magmatic events related to the breakup of Rodinia (Zheng YF et al., 2008). It has been reported that the sedimentary environment of SCB evolved from shallow seas to slope facies during the Precambrian to the Early Paleozoic (Shu LS et al., 2021). Additionally, there is no evidence for the development of oceanic crust such as MORB-type basalts in the SCB after about 810 Ma. Therefore, the geochemical characteristics observed in passive continental margin types in this study suggest a tectonic setting corresponding to an initial rift stage of development of Atlantic-type rifted continental

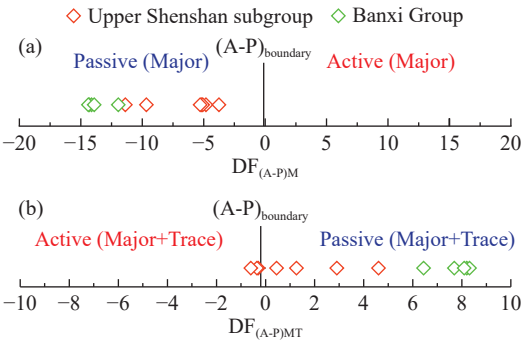

Fig. 10. Individual major elements (a) and combined major and trace elements (b) based multidimensional discriminant function diagram for the metasedimentary samples from the upper Shenshan subgroup and Banxi Group (after Verma SP and Armstrong AJS. 2016).

margins. This suggests a period characterized by intracontinental rifts potentially associated with crustal subsidence (Fig. 11). Subsequently, rift activity in the SCB ceased without the formation of ocean crust, resembling a developmental stage analogous to the contemporary East African Rift (Mapila PH et al., 2009). The reasons for the termination of the rift require further investigation.

6.2. Subdivision of the Shenshan Group

The Shenshan Group is proposed to be redivided into the upper and lower sections for their significant disparities in lithology, sedimentary geochronology, as well as igneous geochemistry and geochronology.

Regarding lithology, notable differences are evident between the two subgroups. The lower section predominantly comprises fine-grained spilites, volcanic breccias, volcanoclastic rocks, and carbonate rocks. The fine-grained spilites often exhibit gray-black siliceous bands and nodules. The upper section is characterized by metabasalts, schists, quartz keratophyres and argillaceous tuffaceous rocks. Lens-shaped bodies of amphibolite, plagioclase-rich rocks, and mafic-ultramafic rocks can also be observed in the upper Shenshan subgroup (Jiangxi BGMR, 1984; Yang X et al., 2022). The lithological distinction is prominent, with the upper section normally exhibiting characteristics of metavolcanic rocks distinct from those of the lower section.

In terms of the sedimentary rocks, distinct differences in detrital zircon geochronological characteristics have been identified. For the upper Shenshan subgroup, our sedimentary rocks gave detrital ages of 810–735 Ma. Wang LJ et al. (2020) reported a minimum peak age of 784–774 Ma for the turbidite. A number of similar youngest apparent detrital ages (776–773 Ma) was given by samples from the sedimentary sequence in the Xiangshan region (Guo FS et al., 2018). With respect to the lower Shenshan subgroup, Yang X (2022) reported a minimum peak age of about 838 Ma for detrital zircons from the sandstone sample. Wang LJ et al. (2022) gave an age of about 853 Ma for the tuffaceous shale. Wang KX et al. (2020) reported the youngest detrital zircon peak age of sedimentary rocks as about 831 Ma. In addition, there are also significant differences in the detrital zircon spectra distribution. The samples from the upper Shenshan subgroup contain a high proportion of ancient zircons, showing two higher peaks in the detrital zircon spectrum of about 2.0 Ga and about 2.5 Ga. On the contrary, the lower Shenshan subgroup mainly containsin an obvious single-peak distribution of about 840 Ma (Yang X, 2022).

Regarding the ages of igneous rocks in the Shenshan Group, published data reveal varying ages for different subgroups. For instance, potassic granite in southern Jiangxi has been dated to about 774 Ma and about 756 Ma (Zhou BW et al., 2018). The Xinyu diorite is attributed to an OIB-type intra-plate basalt with an age of 791±9 Ma, formed in a post-collisional extensional setting, similar to the Banxi Group (Wang YJ et al., 2019). Conversely, the high-Mg volcanic rocks in the lower Shenshan Group are proposed to originate from a sediment-modified wedge source with an age of 839–837 Ma, believed to be equivalent to the Zhoutan, and lower Yingyangguan groups, representing a fore-arc basin property (Yang X et al., 2022).

Based on petrological and chronostratigraphic evidence, the Shenshan Group is discernibly stratified into the lower and upper Shenshan subgroups. The lower Shenshan subgroup is deemed equivalent to the Zhoutan Group, indicating a fore-arc basin setting during the Early Neoproterozoic subduction of the Proto-Huanan Ocean (Yang X et al., 2022). Furthermore, the upper Shenshan subgroup exhibits weathering and source rock characteristics, formation time, and tectonic setting of highly reminiscent of the Banxi Group. They are classified as

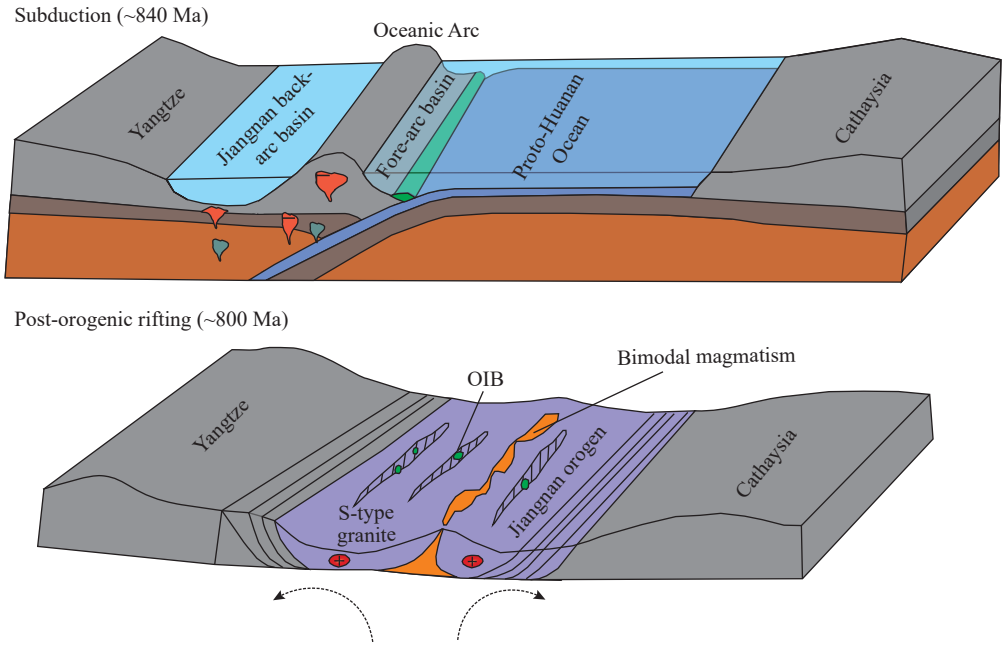

Fig. 11. Schematic cartoon showing the tectonic pattern of Jiangnan Orogen between the Yangtze and Cathysia domains in South China.

equivalent stratigraphic units and imply a Neoproterozoic post-orogenic intracontinental rift setting.

7. Conclusions

(i) The deposition age of the upper Shenshan subgroup spans from 810 Ma to 735 Ma, showing affinity with the Yangtze Domain. The Banxi Group is deposited between 810 and 720 Ma, suggesting sources derived from both the Yangtze and Cathaysia domains.

(ii) Both the upper Shenshan subgroup and Banxi Group experienced moderate chemical weathering under warm and humid conditions. They originated from sedimentary rocks sourced dominated by intermediate to acidic volcanic rocks. The provenance of the upper Shenshan subgroup primarily originates from the Yangtze Domain, while the Banxi Group receives contributions from both the Yangtze and Cathaysia domains.

(iii) The upper Shenshan subgroup and Banxi Group were deposited in a post-orogenic extensional rift setting, which ceased during the Middle Neoproterozoic without formation of ocean crust.

(iv) The previously defined Shenshan Group should be redivided into the upper and lower subgroups, with the upper equivalent to the Banxi Group and lower to the Zhoutan Group.

CRediT authorship contribution statement

Hong-shuai Wu and Yu-zhi Zhang contributed to experiment proposal; Yu-zhi Zhang and Jian-wen Yang contributed to funding acquisition; Hong-shuai Wu, Yu-zhi Zhang and Xue Yang contributed to preliminary research; Hong-shuai Wu, Xue Yang and Cheng Wang contributed to data collection; Hong-shuai Wu, Yu-zhi Zhang, Meng-yuan Li, Cheng-shi Gan contributed to experimental design and analysis; Hong-shuai Wu and Yu-zhi Zhang contributed to writing the original manuscript, writing-review and editing. All authors have read and agreed to the published version of the manuscript.

Declaration of competing interest

The authors declare no conflicts of interest.

Acknowledgement

This study was financially supported by the National Natural Science Foundation of China (42372250, 42102262 and 41972235), National Key Research and Development Program Project (2023YFF0803701), Southern Marine Science and Engineering Guangdong Laboratory (Zhuhai) (SML2023SP206) and the program of China Scholarship Council. We are grateful to Prof. Jin-long Yao and another anonymous reviewer for their constructive reviews and insightful suggestions. This paper is a contribution to Sun Yat-sen University and the University of Windsor.

Supplementary dataset

Supplementary data (Tables S1–S3; Fig. S1) to this article can be found online at doi: 10.31035/cg2024018.

References

Alireza P, Grant MY, Robert HR. 1999. Behavior of major and trace elements (including REE) during Paleoproterozoic pedogenesis and diagenetic alteration of an Archean granite near Ville Marie, Que´bec, Canada. Geochimica et Cosmochimica Acta, 64(13), 2199–2220. doi: 10.1016/S0016-7037(99)00420-2.

Bhatia MR. 1983. Plate tectonics and geochemical composition of sandstones. The Journal of Geology, 91(6), 611–627. doi: 10.1086/628815.

Bhatia MR, Crook KAW. 1986. Trace element characteristics of graywackes and tectonic setting discrimination of sedimentary basins. Contributions to Mineralogy and Petrology, 92(2), 181–193. doi: 10.1007/BF00375292.

Cawood PA, Hawkesworth CJ, Dhuime B. 2012. Detrital zircon record and tectonic setting. Geology, 40(10), 875–878. doi: 10.1130/g32945.1.

Chen K, Gao S, Wu YB, Guo JL, Hu ZC, Liu YS, Zong KQ, Liang ZW, Geng XL. 2013.2.6–2.7Ga crustal growth in Yangtze craton, South China. Precambrian Research, 224, 472–490. doi: 10.1016/j.precamres.2012.10.017.

Chen Q, Sun M, Long XP, Zhao GC, Yuan C. 2016. U–Pb ages and Hf isotopic record of zircons from the late Neoproterozoic and Silurian–Devonian sedimentary rocks of the western Yangtze Block: Implications for its tectonic evolution and continental affinity. Gondwana Research, 31, 184–199. doi: 10.1016/j.gr.2015.01.009.

Condie KC. 1993. Chemical composition and evolution of the upper continental crust: Contrasting results from surface samples and shales. Chemical Geology, 104(1–4), 1–37. doi: 10.1016/0009-2541(93)90140-E.

Cui X, Zhu WB, Ge RF. 2014. Provenance and crustal evolution of the northern Yangtze Block revealed by detrital zircons from Neoproterozoic–early Paleozoic sedimentary rocks in the Yangtze gorges area, South China. The Journal of Geology, 122(2), 217–235. doi: 10.1086/674801.

Dickinson WR, Beard LS, Brakenridge GR, Erjavec JL, Ferguson RC, Inman KF, Knepp RA, Lindberg FA, Ryberg PT. 1983. Provenance of North American Phanerozoic sandstones in relation to tectonic setting. Geological Society of America Bulletin, 94(2), 222. doi: 10.1130/0016-7606(1983)94<222:PONAPS>2.0.CO;2.

Dickinson WR, Gehrels GE. 2009. Use of U–Pb ages of detrital zircons to infer maximum depositional ages of strata: A test against a Colorado Plateau Mesozoic database. Earth and Planetary Science Letters, 288(1-2), 115–125. doi: 10.1016/j.epsl.2009.09.013.

Dostal J, Chatterjee AK. 2000. Contrasting behaviour of Nb/Ta and Zr/Hf ratios in a peraluminous granitic pluton (Nova Scotia, Canada). Chemical Geology, 163(1–4), 207–218. doi: 10.1016/S0009-2541(99)00113-8.

Duan Z, Xing GF, Liao SB, Chu PL, Huang WC, Zhu YH, Shu XJ, Li CB. 2018. Petrogenesis of the microcrystalline-dioritic enclaves from Jiuling granitoids in the eastern segment of Jiangnan Orogen and constraints on magma source materials. China Geology, 2(3), 374–391. doi: 10.31035/cg2018042.

Falvey DA. 1974. The Development of Continental Margins in Plate Tectonic Theory. The APPEA Journal, 14(1), 95–106. https://www.publish.csiro.au/AJ/AJ73012.

Floyd PA, Leveridge BE. 1987. Tectonic environment of the Devonian Gramscatho basin, south Cornwall: Framework mode and

geochemical evidence from turbiditic sandstones. Journal of the Geological Society, 144(4), 531–542. doi: 10.1144/gsjgs.144.4.0531.

Floyd PA, Shail R, Leveridge BE, Franke W. 1991. Geochemistry and provenance of rhenohercynian synorogenic sandstones: Implications for tectonic environment discrimination. Geological Society of London Special Publications, 57(1), 173–188. doi: 10.1144/GSL.SP.1991.057.01.14.

Gan CS, Wang YJ, Sheldrick TC, Qian X, Zhang YZ. 2024. Spatio-temporal framework of the Jurassic mafic rocks in South China: Implications for two stages of intra-continental extension. Lithos, 466, 107456. doi: 10.1016/j.lithos.2023.107456.

Gao LZ, Chen J, Ding XZ, Liu YR, Zhang CH, Zhang H, Liu XY, Pang WH, Zhang YH. 2011. Zircon SHRIMP U‑Pb Dating of the Tuff Bed of Lengjiaxi and Banxi Groups, Northeastern Hunan: Constraints on the Wuling Movement. Geological Bulletin of China, 30(7), 1001–1008 (in Chinese with English abstract). doi: 10.12097/gbc.20110701.

Gao LZ, Ding XZ, Liu YX, Zhang CH, Zhang H, Huang ZZ, Xu XM, Zhou ZY. 2014. SHRIMP zircon U-Pb dating of Neoproterozoic Chencai Complex in Jiangshan- Shaoxing fault zone and its implications. Geological Bulletin of China, 33(5), 641–648 (in Chinese with English abstract). https://webofscience.clarivate.cn/wos/alldb/full-record/CSCD:5163236.

Green TH. 1994. Experimental studies of trace-element partitioning applicable to igneous petrogenesis—Sedona 16 years later. Chemical Geology, 117(1-4), 1–36. doi: 10.1016/0009-2541(94)90119-8.

Greentree MR, Li ZX, Li XH, Wu HC. 2006. Late Mesoproterozoic to earliest Neoproterozoic basin record of the Sibao orogenesis in western South China and relationship to the assembly of Rodinia. Precambrian Research, 151(1–2), 79–100. doi: 10.1016/j.precamres.2006.08.002.

Guo FS, Shi G, Yang QK, Zhang WL, Xie CF, Zhou WP, Zhang JW. 2018. Timing of metamorphism and provenance of the metamorphic basement of the Xiangshan Uranium Orefield, Jiangxi Province, China. Acta Geologica Sinica-English Edition, 92, 34–55. doi: 10.1111/1755-6724.13493.

Hofmann M, Linnemann U, Rai V, Becker S, Gärtner A, Sagawe A. 2011. The India and South China cratons at the margin of rodinia—Synchronous Neoproterozoic magmatism revealed by LA-ICP-MS zircon analyses. Lithos, 123(1–4), 176–187. doi: 10.1016/j.lithos.2011.01.012.

Hoskin PWO. 2003. The composition of zircon and igneous and metamorphic petrogenesis. Reviews in Mineralogy and Geochemistry, 53(1), 27–62. doi: 10.2113/0530027.

Hugh R Rollinson. 1993. Using Geochemical Date: Evaluation, Presentation, Interpretation. London (Longman Scientific and Technical). 384. doi: 10.4324/9781315845548.

Hunan BGMR (Bureau of Geology and Mineral Resources of Hunan Province). 1988. Regional Geology of Hunan Province. Geological Publishing House, Beijing (in Chinese).

Jiangxi BGMR (Bureau of Geology and Mineral Resources of Jiangxi province). 1984. Regional Geology of Jiangxi Province. Geological Publishing House, Beijing (in Chinese).

Jiang Y, Zhao XL, Zhang YJ, Xing GF, Xu MC, Liu H. 2019. Neoproterozoic arc volcanic rocks of the Nanping–Ninghua tectonic belt, South China: Implications for the collision between the North and South Wuyi blocks. Geological Journal, 54(4), 2679–2692. doi: 10.1002/gj.3318.

Lan ZW, Li XH, Zhu MY, Zhang QR, Li QL. 2015. Revisiting the Liantuo formation in Yangtze Block, South China: SIMS U–Pb zircon age constraints and regional and global significance. Precambrian Research, 263, 123–141. doi: 10.1016/j.precamres.2015.03.012.

Li WX, Li XH, Li ZX. 2005. Neoproterozoic bimodal magmatism in the Cathaysia Block of South China and its tectonic significance. Precambrian Research, 136(1), 51–66. doi: 10.1016/j.precamres.2004.09.008.

Li XH. 1999. U–Pb zircon ages of granites from the southern margin of the Yangtze Block: Timing of Neoproterozoic Jinning: Orogeny in SE China and implications for Rodinia Assembly. Precambrian Research, 97(1-2), 43–57. doi: 10.1016/S0301-9268(99)00020-0.

Li XH, Li WX, He B. 2012. Building of the South China Block and its relevance to assembly and breakup of Rodinia supercontinent: Observations, interpretations and tests. Bulletin of Mineralogy, Petrology and Geochemistry, 31(6), 543–559. doi: 10.3969/j.issn.1007-2802.2012.06.002.

Li ZX, Zhang LH, Powell CM. 1995. South China in rodinia: Part of the missing link between Australia–east Antarctica and laurentia? Geology, 23(5), 407. doi: 10.1130/0091-7613(1995)023<0407:scirpo>2.3.co;2.

Li ZX, Liu YB, Ernst R. 2023. A dynamic 2000–540 Ma earth history: From cratonic amalgamation to the age of supercontinent cycle. Earth-Science Reviews, 238, 104336. doi: 10.1016/j.earscirev.2023.104336.

Lin SF, Xing GF, Davis DW, Yin CQ, Wu ML, Li LM, Jiang Y, Chen ZH. 2018. Appalachian-style multi-terrane Wilson cycle model for the assembly of South China. Geology, 46(4), 319–322. doi: 10.1130/g39806.1.

Liu XM, Gao S, Diwu CR, Ling WL. 2008. Precambrian crustal growth of Yangtze Craton as revealed by detrital zircon studies. American Journal of Science, 308(4), 421–468. doi: 10.2475/04.2008.02.

Mapila PH, Tiercelin JJ, Benoit M, Ringrose S, Diskin S, Cotten J, Hémond C. 2009. Sediment geochemistry and tectonic setting: Application of discrimination diagrams to early stages of intracontinental rift evolution, with examples from the Okavango and southern Tanganyika Rift basins. Journal of African Earth Sciences, 53(1-2), 33–44. doi: 10.1016/j.jafrearsci.2008.07.005.

McLennan SM, McCulloch MT, Taylor SR, Maynard JB. 1989. Effects of sedimentary sorting on neodymium isotopes in deep-sea turbidites. Nature, 337(6207), 547–549. doi: 10.1038/337547a0.

Nesbitt H, Markovics G. 1997. Weathering of granodioritic crust, long-term storage of elements in weathering profiles, and petrogenesis of siliciclastic sediments. Geochimica et Cosmochimica Acta, 61(8), 1653–1670. doi: 10.1016/S0016-7037(97)00031-8.

Nesbitt HW, Young GM. 1982. Early Proterozoic climates and plate motions inferred from major element chemistry of lutites. Nature, 299, 715–717. doi: 10.1038/299715a0.

Pan GT, Lu SN, Xiao QH, Zhang KX, Yin FG, Hao GJ, Luo MS, Ren F, Yuan SH. 2016. Division of tectonic stages and tectonic evolution in China. Earth Science Frontiers, 23(06), 1–23. doi: 10.13745/j.esf.2016.06.001.

Pettijohn FJ, Potter PE, Siever R. 1972. Sand and Sandstone. Springer, New York. doi: 10.1016/0012-8252(72)90066-9.

Robert LC, Victor NP. 2002. The source and origin of terrigenous sedimentary rocks in the Mesoproterozoic Ui group, southeastern Russia. Precambrian Research, 117, 157–183. doi: 10.1016/S0301-9268(02)00079-7.

Ronadh C, Donald RL, Cullers RL. 1995. The influence of sediment recycling and basement composition on evolution of mudrock chemistry in the southwestern United States. Geochimica et Cosmochimica Acta, 59(14), 2919–2940. doi: 10.1016/0016-7037(95)00185-9.

Roser BP, Korsch RJ. 1988. Provenance signatures of sandstone-mudstone suites determined using discriminant function analysis of major-element data. Chemical Geology, 67(1–2), 119–139. doi: 10.1016/0009-2541(88)90010-1.

Shu LS, Yao JL, Wang B, Faure M, Charvet J, Chen Y. 2021. Neoproterozoic plate tectonic process and Phanerozoic geodynamic

evolution of the South China Block. Earth-Science Reviews, 216, 103596. doi: 10.1016/j.earscirev.2021.103596.

Sun SS, McDonough WF. 1989. Chemical and isotopic systematics of oceanic basalts: Implications for mantle composition and processes. Geological Society of London Special Publications, 42(1), 313–345. doi: 10.1144/GSL.SP.1989.042.01.19.

Sun WH, Zhou MF, Gao JF, Yang YH, Zhao XF, Zhao JH. 2009. Detrital zircon U–Pb geochronological and Lu–Hf isotopic constraints on the Precambrian magmatic and crustal evolution of the western Yangtze Block, SW China. Precambrian Research, 172(1–2), 99–126. doi: 10.1016/j.precamres.2009.03.010.

Taylor SR, McLennan SM. 1985. The Continental Crust: Its composition and Evolution, An Examination of the Geochemical Record Preserved in Sedimentary Rocks. Blackwell Scientific Publications, Oxford London. https://xueshu.baidu.com/usercenter/paper/show?paperid=dfaf1e11602387cf62b5a3ab97478ff4&site=xueshu_se&hitarticle=1.

Verma SP, Armstrong-Altrin JS. 2016. Geochemical discrimination of siliciclastic sediments from active and passive margin settings. Sedimentary Geology, 332, 1–12. doi: 10.1016/j.sedgeo.2015.11.011.

Wan YS, Liu DY, Xu MH, Zhuang JM, Song B, Shi YR, Du LL. 2007. SHRIMP U–Pb zircon geochronology and geochemistry of metavolcanic and metasedimentary rocks in Northwestern Fujian, Cathaysia block, China: Tectonic implications and the need to redefine lithostratigraphic units. Gondwana Research, 12(1–2), 166–183. doi: 10.1016/j.gr.2006.10.016.

Wang J, Li XH, Duan TZ, Liu DY, Song B, Li ZX, Gao YH. 2003. Zircon SHRIMP U — Pb dating for the Cangshuipu volcanic rocks and its implications for the lower boundary age of the Nanhua Strata in South China. Chinese Science Bulletin, 48(16), 1726–1731. doi: 10.1360/03wd0168.

Wang JQ, Shu LS, Santosh M. 2017. U-Pb and Lu-Hf isotopes of detrital zircon grains from Neoproterozoic sedimentary rocks in the central Jiangnan Orogen, South China: Implications for Precambrian crustal evolution. Precambrian Research, 294, 175–188. doi: 10.1016/j.precamres.2017.03.025.

Wang KX, Sun LQ, Sun T, Huang H. 2020. Depositional age, provenance, and tectonic implications of Neoproterozoic sedimentary rocks in the Xiangshan area, South China. Geological Journal, 56(3), 1584–1603. doi: 10.1002/gj.4000.

Wang LJ, Zhang KX, Lin SF, He WH, Kou XH, Zhou XH. 2020. Turbidite record of a middle Neoproterozoic active continental margin in the West Cathaysia terrane, South China: Implications for the relationships between the Yangtze and Cathaysia blocks and their positions in Rodinia. Precambrian Research, 337, 105457. doi: 10.1016/j.precamres.2019.105457.

Wang LJ, Zhang KX, Lin SF, He WH, Yin LM. 2022. Origin and age of the Shenshan tectonic mélange in the Jiangshan-Shaoxing-Pingxiang Fault and late Early Paleozoic juxtaposition of the Yangtze Block and the West Cathaysia terrane, South China. GSA Bulletin, 134(1-2), 113–129. doi: 10.1130/b35963.1.

Wang PM, Yu JH, Sun T, Ling HF, Chen PR, Zhao KD, Chen WF, Liu Q. 2012. Geochemistry and detrital zircon geochronology of Neoproterozoic sedimentary rocks in Eastern Hunan Province and their tectonic significance. Acta Petrologica Sinica, 28(12), 3841–3857. https://webofscience.clarivate.cn/wos/alldb/full-record/WOS:000313315700005 (in Chinese with English abstract).

Wang PM, Yu JH, Sun T, Shi Y, Chen PR, Zhao KD, Chen WF, Liu Q. 2013. Composition variations of the Sinian-Cambrian sedimentary rocks in Hunan and Guangxi provinces and their tectonic significance. Scientia Sinica(Terrae), 11(43), 1893–1906 (in Chinese with English abstract). doi: 10.1007/s11430-013-4634-1.

Wang W, Zhou MF. 2012. Sedimentary records of the Yangtze Block (South China) and their correlation with equivalent Neoproterozoic sequences on adjacent continents. Sedimentary Geology, 265, 126–142. doi: 10.1016/j.sedgeo.2012.04.003.

Wang W, Zhou MF, Yan DP, Li L, Malpas J. 2013. Detrital zircon record of Neoproterozoic active-margin sedimentation in the eastern Jiangnan Orogen, South China. Precambrian Research, 235, 1–19. doi: 10.1016/j.precamres.2013.05.013.

Wang XL, Shu LS, Xing GF, Zhou JC, Tang M, Shu XJ, Qi L, Hu YH. 2012. Post-orogenic extension in the eastern part of the Jiangnan orogen: Evidence from ca 800–760Ma volcanic rocks. Precambrian Research, 222, 404–423. doi: 10.1016/j.precamres.2011.07.003.

Wang XL, Zhou JC, Griffin WL, Zhao GC, Yu JH, Qiu JS, Zhang YJ, Xing GF. 2014. Geochemical zonation across a Neoproterozoic Orogenic Belt: Isotopic evidence from granitoids and metasedimentary rocks of the Jiangnan Orogen, China. Precambrian Research, 242, 154–171. doi: 10.1016/j.precamres.2013.12.023.

Wang YJ, Gan CS, Tan QL, Zhang YZ, He HY, Xin Q, Zhang YH. 2018. Early Neoproterozoic (about 840 Ma) slab window in South China: Key magmatic records in the Chencai complex. Precambrian Research, 314, 434–451. doi: 10.1016/j.precamres.2018.06.002.

Wang YJ, Zhang AM, Cawood PA, Fan WM, Xu JF, Zhang GW, Zhang YZ. 2013. Geochronological, geochemical and Nd–Hf–Os isotopic fingerprinting of an early Neoproterozoic arc–back-arc system in South China and its accretionary assembly along the margin of Rodinia. Precambrian Research, 231, 343–371. doi: 10.1016/j.precamres.2013.03.020.

Wang YJ, Zhang YZ, Cawood PA, Wang C, Gan CS. 2024. Proterozoic tectonics of eastern South China: From Ca. 1.45 Ga rifting in the interior of Columbia to a long-lived convergent orogen at the periphery of rodinia. Earth-Science Reviews, 249, 104652. doi: 10.1016/j.earscirev.2023.104652.

Wang YJ, Zhang YZ, Cawood PA, Zhou YZ, Zhang FF, Yang X, Cui X. 2019. Early Neoproterozoic assembly and subsequent rifting in South China: Revealed from mafic and ultramafic rocks, central Jiangnan Orogen. Precambrian Research, 331, 105367. doi: 10.1016/j.precamres.2019.105367.

Watson EB, Harrison TM. 1984. Accessory minerals and the geochemical evolution of crustal magmatic systems: A summary and prospectus of experimental approaches. Physics of the Earth and Planetary Interiors, 35(1–3), 19–30. doi: 10.1016/0031-9201(84)90031-1.

Wollast R, Chou L. 1992. Surface reactions during the early stages of weathering of albite. Geochimica et Cosmochimica Acta, 56(8), 3113–3121. doi: 10.1016/0016-7037(92)90292-Q.

Wu FY, Li XH, Zheng YF, Gao S. 2007. Lu-Hf isotopic systematics and their applications in petrology. Acta Petrologica Sinica, 23(2), 185–220. doi: 10.3969/j.issn.1000-0569.2007.02.001.

Wu H, Jiang XS, Wang J, Wang ZJ, Du QD, Deng Q, Cui XZ, Yang F. 2013. Ages and provenance of Neoproterozoic Dajiangbian Formation and Aiqiling Formation in southeast Hunan Province: U-Pb geochronological evidence of detrital zircons. Geological Review, 59, 853–868. doi: 10.16509/j.georeview.2013.05.021.

Wu L, Jia D, Li HB, Deng F, Li YQ. 2010. Provenance of detrital zircons from the late Neoproterozoic to Ordovician sandstones of South China: Implications for its continental affinity. Geological Magazine, 147(6), 974–980. doi: 10.1017/s0016756810000725.

Wu RX, Zheng YF, Wu YB, Zhao ZF, Zhang SB, Liu XM, Wu FY. 2006. Reworking of juvenile crust: Element and isotope evidence from Neoproterozoic granodiorite in South China. Precambrian Research, 146(3-4), 179–212. doi: 10.1016/j.precamres.2006.01.012.

Xu XB, Zhang YQ, Shu LS, Jia D, Wang RR, Xu HZ. 2010. Precambrian geochronology and stratigraphy in the Wuyishan Area, South China. Journal of Stratigraphy, 34, 254–267 (in Chinese with English abstract). doi: 10.19839/j.cnki.dcxzz.2010.03.004.

Yang X, Wang YJ, Zhang YZ, Gan CS, Qian X. 2022. Early

Neoproterozoic (~840 Ma) assemblage in South China and the southern extension of the Jiangshan-Shaoxing zone: Records from the Zhoutan and Shenshan igneous rocks in central Jiangxi. Precambrian Research, 371, 106573. doi: 10.1016/j.precamres.2022.106573.

Yang X. 2022. Early Neoproterozoic Assemblage in South China: Records from the Magmatism and Sedimentation in Hunan and Jiangxi Provinces. Sun Yat-sen University, Zhuhai (in Chinese with English abstract).

Yao JL, Cawood PA, Shu LS, Zhao GC. 2019. Jiangnan Orogen, South China: A about 970–820 Ma Rodinia margin accretionary belt. Earth-Science Reviews, 196, 102872. doi: 10.1016/j.earscirev.2019.05.016.

Yu JH, O'Reilly SY, Wang LJ, Griffin WL, Zhang M, Wang RC, Jiang SY, Shu LS. 2008. Where was South China in the rodinia supercontinent? Precambrian Research, 164(1–2), 1–15. doi: 10.1016/j.precamres.2008.03.002.

Yu JH, O'Reilly SY, Wang LJ, Griffin WL, Zhou MF, Zhang M, Shu LS. 2010. Components and episodic growth of Precambrian crust in the cathaysia block, South China: Evidence from U–Pb ages and Hf isotopes of zircons in Neoproterozoic sediments. Precambrian Research, 181(1–4), 97–114. doi: 10.1016/j.precamres.2010.05.016.

Yu PP, Zhang YZ, Zhou YZ, Weinberg RF, Zheng Y, Yang WB. 2019. Melt evolution of crustal anatexis recorded by the Early Paleozoic Baiyunshan migmatite-granite suite in South China. Lithos, 332, 83–98. doi: 10.1016/j.lithos.2019.02.020.

Zhang QR, Li XH, Feng LJ, Huang J, Song B. 2008. A new age constraint on the onset of the Neoproterozoic glaciations in the Yangtze platform, South China. The Journal of Geology, 116(4), 423–429. doi: 10.1086/589312.

Zhang YZ, Wang YJ, Geng HY, Zhang YH, Fan WM, Zhong H. 2013. Early Neoproterozoic (~850 Ma) back-arc basin in the central Jiangnan Orogen (eastern South China): Geochronological and petrogenetic constraints from meta-basalts. Precambrian Research, 231, 325–342. doi: 10.1016/j.precamres.2013.03.016.

Zhang YZ, Wang YJ, Zhang YH, Zhang AM. 2015. Neoproterozoic assembly of the Yangtze and cathaysia blocks: Evidence from the cangshuipu group and associated rocks along the central Jiangnan Orogen, South China. Precambrian Research, 269, 18–30. doi: 10.1016/j.precamres.2015.08.003.

Zhang YZ, Wang YJ. 2016. Early Neoproterozoic (~840Ma) arc magmatism: Geochronological and geochemical constraints on the metabasites in the central Jiangnan Orogen. Precambrian Research, 275, 1–17. doi: 10.1016/j.precamres.2015.11.006.

Zhang YZ, Wang YJ. 2020. Early Neoproterozoic continental arc system at the central Jiangnan Orogen, South China: Geochronological and geochemical constraints on the key igneous rock-association. GSA Bulletin, 132(3-4), 638–654. doi: 10.1130/b35221.1.

Zhao GC. 2015. Jiangnan orogen in South China: Developing from divergent double subduction. Gondwana Research, 27(3), 1173–1180. doi: 10.1016/j.gr.2014.09.004.

Zhao GC, Cawood PA. 2012. Precambrian geology of China. Precambrian Research, 222–223, 13–54. doi: 10.1016/j.precamres.2012.09.018.

Zhao JH, Zhou MF, Yan DP, Zheng JP, Li JW. 2011. Reappraisal of the ages of Neoproterozoic strata in South China: No connection with the grenvillian orogeny. Geology, 39(4), 299–302. doi: 10.1130/G31701.1.

Zheng Y, Long LJ, Yu PP, Zhang XC, Hu ZB, Wu YH. 2022. Metal endowment and geodynamic evolution of the Late Paleozoic SEDEX deposits in South China: The Yunfu giant iron-sulfide deposit, Yunkai Domain. Ore Geology Reviews, 145, 104918. doi: 10.1016/j.oregeorev.2022.104918.

Zheng YF, Wu RX, Wu YB, Zhang SB, Yuan HL, Wu FY. 2008. Rift melting of juvenile arc-derived crust: Geochemical evidence from Neoproterozoic volcanic and granitic rocks in the Jiangnan Orogen, South China. Precambrian Research, 163(3–4), 351–383. doi: 10.1016/j.precamres.2008.01.004.

Zheng YF, Zhang SB, Zhao ZF, Wu YB, Li XH, Li ZX, Wu FY. 2007. Contrasting zircon Hf and O isotopes in the two episodes of Neoproterozoic granitoids in South China: Implications for growth and reworking of continental crust. Lithos, 96(1–2), 127–150. doi: 10.1016/j.lithos.2006.10.003.

Zhou BW, Zeng GF, Xu WT, Feng YX. 2018. The discovery of Early Nanhuan K-bentonite in southern Jiangxi and its tectonic significance. Journal of Geology, 42(1), 95–107(in Chinese with English abstract).

Zhou JC, Wang XL, Qiu JS. 2009. Geochronology of Neoproterozoic mafic rocks and sandstones from northeastern Guizhou, South China: Coeval arc magmatism and sedimentation. Precambrian Research, 170(1–2), 27–42. doi: 10.1016/j.precamres.2008.11.002.

Zhou MF, Yan DP, Kennedy AK, Li YQ, Ding J. 2002. SHRIMP U–Pb zircon geochronological and geochemical evidence for Neoproterozoic arc-magmatism along the western margin of the Yangtze Block, South China. Earth and Planetary Science Letters, 196(1–2), 51–67. doi: 10.1016/S0012-821X(01)00595-7.